MODELING STATICS AND DYNAMICS OF MILLING MACHINE COMPONENTS

by
EVREN BURCU KIVANÇ

Submitted to the Graduate School of Engineering and Natural Sciences
in partial fulfillment of
the requirements for the degree of
Master of Science

Sabancı University
July 2003

MODELING STATICS AND DYNAMICS

OF MILLING MACHINE COMPONENTS

APPROVED BY:

Assistant Prof. Dr. Erhan Budak …….

(Thesis Advisor)

Assistant Prof. Dr. İsmail Lazoğlu …….

Assistant Prof. Dr. Bülent Çatay …….

DATE OF APPROVAL: …….

ACKNOWLEDGEMENTS

It is a pleasure to thank the many people who made this thesis possible.

I thank Assistant Prof. Dr. Erhan Budak for his continuous guidance, motivation and patience from beginning to end. He manages to strike the perfect balance between providing direction and encouraging independence.

I would generously like to thank graduate committee members of my thesis, for their critical suggestions and excellent remarks on my thesis.

I am grateful to *Özkan Öztürk* who has assisted me during my whole study. *Özkan Öztürk* has been particularly helpful and generous with their time and expertise during this project. Thanks for those long hours we spent working on modal analysis test… Thank you for your support and encouragement.

I also wish to acknowledge all the faculty members, graduate students and other staff of Sabanci University who have been made this thesis possible to conclude. Special thanks to my love *Onur Devran Çakır*, *Bilge Küçük*, *Şilan Hun, Mehmet Kayhan*, *Çağdas Arslan, Bülent Delibaş* and my roommate *Ece Gamsız* for helping me get through the difficult times and for all the emotional support, comradeship, entertainment, and caring they provided.

I wish to thank my entire extended family for providing a loving environment for me. My parents have always encouraged me and guided me to independence, never trying to limit my aspirations. I am grateful to them and amazed at their generosity.

ABSTRACT

CAD/CAM systems and CNC machine tools have made significant impact on machining accuracy and productivity. However, material removal rate and quality in machining may still be limited due to issues related to the process mechanics which are not considered in CAD/CAM systems. In this study, modeling structural properties of milling system components is presented. These models eliminate the need for stiffness and transfer function measurements, and together with cutting force and stability models, they can be integrated into CAD/CAM systems to predict and compensate surface errors, and determine chatter free machining conditions. Therefore, the process is also simulated in addition to the geometry, which is usually the missing part in virtual manufacturing systems. The goal of this research is to develop a virtual machining system for precision machining of sculptured surfaces in which the part geometric errors contributed by the machine tool errors are predicted and evaluated prior to the real cutting.

Cutting forces produce deformations of the tool and these cause dimensional and form errors on the workpiece. Milling forces can be modeled for given cutter geometry, cutting conditions and work material. The force prediction can be used to determine form errors on the finished surface. Chatter vibrations developed due to dynamic interactions between the cutting tool and workpiece. Chatter vibrations cause poor surface finish and inconsistent product quality. Static and dynamic properties of end mill are required to predict the form errors and chatter stability limits without measurement. In this research, generalized equations are presented which can be used for predicting static and dynamic properties of the cutting tool. The static and dynamic characteristics of tool and tool holder can be obtained by using finite element analysis (FEA). Considering great variety of machine tool and tool holder configurations and geometries, FEA for each configuration is very time consuming. In this study, the models are seemed to be accurate for prediction statics and dynamics characteristics of the tool.

ÖZET

Günümüzde CAD/CAM sistemlerinin ve CNC takım tezgahlarının kullanımının artması ile işleme hassasiyetinde ve verimlilikte önemli gelişmeler elde edilmiştir. Ancak talaş kaldırma oranı ve kalite gibi işleme mekaniğine bağımlı konular hala CAD/CAM sistemlerinde göz ardı edilmektedir. Bu çalışmada frezeleme sisteminin yapısal özellikleri modellenmiştir. Bu modellerin elastiklik katsayısı ve transfer fonksiyonu ölçümüne gerek kalmadan, kesme kuvveti modelleri ve kararlılık modelleri ile birlikte CAD/CAM sistemlerine katılarak yüzey hatalarının tahmini ve giderilmesi, aynı zamanda tırlama oluşmadan kesme yapılabilmesini sağlar. Bu çalışmada takımlardan dolayı kaynaklanan geometrik hataları kesme yapmadan önce tahmin eden sanal üretim sistemi yapılması amaçlanmıştır.

Kesme kuvvetleri takımda deformasyonlara neden olmakta ve bu deformasyonlardan dolayı ölçü ve şekil hataları meydana gelmektedir. Frezeleme kuvvetleri, kesici takım geometrisi, kesme koşulları ve iş parçası malzesine bağımlı olarak modellenmektedir. Bu modelleme sonucu elde edilen kuvvet tahminleri, işlenmiş yüzeydeki form hatalarının hesaplanmasında kullanılabilir. Tırlama, kesici takım ve iş parçası arasındaki dinamik etkileşimler nedeniyle oluşmaktadır. Tırlama düşük yüzey kalitesine ve istikrarsız ürün kalitesine sebep olur. Parmak frezenin statik ve dinamik özellikleri, form hataları ve tırlama kararlılık sınırlarını ölçmeden tahmin etmek için gereklidir. Bu araştırmada kesici takımın statik ve dinamik özelliklerini tahmin etmekte kullanılabilecek genel denklemler sunulmuştur. Takımın ve takım tutucunun statik ve dinamik karakterleri sonlu elemanlar analizi yöntemi kullanılarak elde edilmiştir. Takım ve takım tutucuların çok çeşitli düzenek ve geometrileri göz önüne alındığında, tamamı için ayrı ayrı sonlu elemanlar analizi yapmak çok zaman alıcı bir iştir. Bu çalışmada elde edilen modellerin statik ve dinamik karakterleri belirlemede doğru sonuçlar verdiği ispatlanmıştır.

TABLE OF CONTENTS

LIST OF FIGURES

LIST OF TABLES

MODELING STATICS AND DYNAMICS OF MILLING MACHINE COMPONENTS

by
EVREN BURCU KIVANÇ

Submitted to the Graduate School of Engineering and Natural Sciences
in partial fulfillment of
the requirements for the degree of
Master of Science

Sabancı University
July 2003

MODELING STATICS AND DYNAMICS

OF MILLING MACHINE COMPONENTS

APPROVED BY:

Assistant Prof. Dr. Erhan Budak …….

(Thesis Advisor)

Assistant Prof. Dr. İsmail Lazoğlu …….

Assistant Prof. Dr. Bülent Çatay …….

DATE OF APPROVAL: …….

ACKNOWLEDGEMENTS

It is a pleasure to thank the many people who made this thesis possible.

I thank Assistant Prof. Dr. Erhan Budak for his continuous guidance, motivation and patience from beginning to end. He manages to strike the perfect balance between providing direction and encouraging independence.

I would generously like to thank graduate committee members of my thesis, for their critical suggestions and excellent remarks on my thesis.

I am grateful to *Özkan Öztürk* who has assisted me during my whole study. *Özkan Öztürk* has been particularly helpful and generous with their time and expertise during this project. Thanks for those long hours we spent working on modal analysis test… Thank you for your support and encouragement.

I also wish to acknowledge all the faculty members, graduate students and other staff of Sabanci University who have been made this thesis possible to conclude. Special thanks to my love *Onur Devran Çakır*, *Bilge Küçük*, *Şilan Hun, Mehmet Kayhan*, *Çağdas Arslan, Bülent Delibaş* and my roommate *Ece Gamsız* for helping me get through the difficult times and for all the emotional support, comradeship, entertainment, and caring they provided.

I wish to thank my entire extended family for providing a loving environment for me. My parents have always encouraged me and guided me to independence, never trying to limit my aspirations. I am grateful to them and amazed at their generosity.

ABSTRACT

CAD/CAM systems and CNC machine tools have made significant impact on machining accuracy and productivity. However, material removal rate and quality in machining may still be limited due to issues related to the process mechanics which are not considered in CAD/CAM systems. In this study, modeling structural properties of milling system components is presented. These models eliminate the need for stiffness and transfer function measurements, and together with cutting force and stability models, they can be integrated into CAD/CAM systems to predict and compensate surface errors, and determine chatter free machining conditions. Therefore, the process is also simulated in addition to the geometry, which is usually the missing part in virtual manufacturing systems. The goal of this research is to develop a virtual machining system for precision machining of sculptured surfaces in which the part geometric errors contributed by the machine tool errors are predicted and evaluated prior to the real cutting.

Cutting forces produce deformations of the tool and these cause dimensional and form errors on the workpiece. Milling forces can be modeled for given cutter geometry, cutting conditions and work material. The force prediction can be used to determine form errors on the finished surface. Chatter vibrations developed due to dynamic interactions between the cutting tool and workpiece. Chatter vibrations cause poor surface finish and inconsistent product quality. Static and dynamic properties of end mill are required to predict the form errors and chatter stability limits without measurement. In this research, generalized equations are presented which can be used for predicting static and dynamic properties of the cutting tool. The static and dynamic characteristics of tool and tool holder can be obtained by using finite element analysis (FEA). Considering great variety of machine tool and tool holder configurations and geometries, FEA for each configuration is very time consuming. In this study, the models are seemed to be accurate for prediction statics and dynamics characteristics of the tool.

ÖZET

Günümüzde CAD/CAM sistemlerinin ve CNC takım tezgahlarının kullanımının artması ile işleme hassasiyetinde ve verimlilikte önemli gelişmeler elde edilmiştir. Ancak talaş kaldırma oranı ve kalite gibi işleme mekaniğine bağımlı konular hala CAD/CAM sistemlerinde göz ardı edilmektedir. Bu çalışmada frezeleme sisteminin yapısal özellikleri modellenmiştir. Bu modellerin elastiklik katsayısı ve transfer fonksiyonu ölçümüne gerek kalmadan, kesme kuvveti modelleri ve kararlılık modelleri ile birlikte CAD/CAM sistemlerine katılarak yüzey hatalarının tahmini ve giderilmesi, aynı zamanda tırlama oluşmadan kesme yapılabilmesini sağlar. Bu çalışmada takımlardan dolayı kaynaklanan geometrik hataları kesme yapmadan önce tahmin eden sanal üretim sistemi yapılması amaçlanmıştır.

Kesme kuvvetleri takımda deformasyonlara neden olmakta ve bu deformasyonlardan dolayı ölçü ve şekil hataları meydana gelmektedir. Frezeleme kuvvetleri, kesici takım geometrisi, kesme koşulları ve iş parçası malzesine bağımlı olarak modellenmektedir. Bu modelleme sonucu elde edilen kuvvet tahminleri, işlenmiş yüzeydeki form hatalarının hesaplanmasında kullanılabilir. Tırlama, kesici takım ve iş parçası arasındaki dinamik etkileşimler nedeniyle oluşmaktadır. Tırlama düşük yüzey kalitesine ve istikrarsız ürün kalitesine sebep olur. Parmak frezenin statik ve dinamik özellikleri, form hataları ve tırlama kararlılık sınırlarını ölçmeden tahmin etmek için gereklidir. Bu araştırmada kesici takımın statik ve dinamik özelliklerini tahmin etmekte kullanılabilecek genel denklemler sunulmuştur. Takımın ve takım tutucunun statik ve dinamik karakterleri sonlu elemanlar analizi yöntemi kullanılarak elde edilmiştir. Takım ve takım tutucuların çok çeşitli düzenek ve geometrileri göz önüne alındığında, tamamı için ayrı ayrı sonlu elemanlar analizi yapmak çok zaman alıcı bir iştir. Bu çalışmada elde edilen modellerin statik ve dinamik karakterleri belirlemede doğru sonuçlar verdiği ispatlanmıştır.

TABLE OF CONTENTS

LIST OF FIGURES

LIST OF TABLES

CHAPTER 1

INTRODUCTION

Milling is one of the most commonly used machining processes in industry. Great variety of parts with different geometry, complexity, quality and materials can be produced by milling. In milling the main cutting motion is the rotation of a multitoothed cutter that machines a workpiece that performs translative feed motions. There are two basic models, face milling and peripheral milling (up and down milling). A very common type of peripheral milling is end milling (Figure 1.1). The geometry of end milling operation is presented in Figure 1.2.

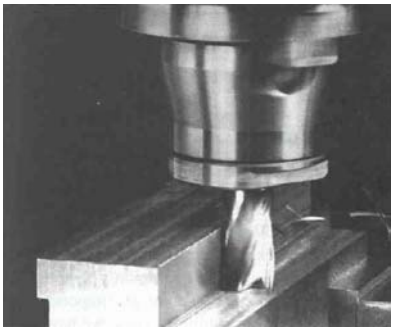

Figure 1.1: End milling operation

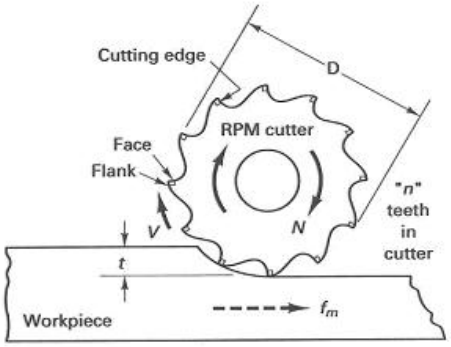

Figure 1.2:Geometry of end milling

Depending on the workpiece geometry, different milling cutters are used. Tool holders are used to provide good concentricity between tool and machine spindle. (Figure 1.3)

Figure 1.3: Various milling cutting tools and tool holders

An end mill is a cutter of a smaller diameter (usually between 5 mm and 30 mm diameter) clamped in overhang, and its length is several times its diameter. Figure 1.4 shows an end mill with detail geometric properties.

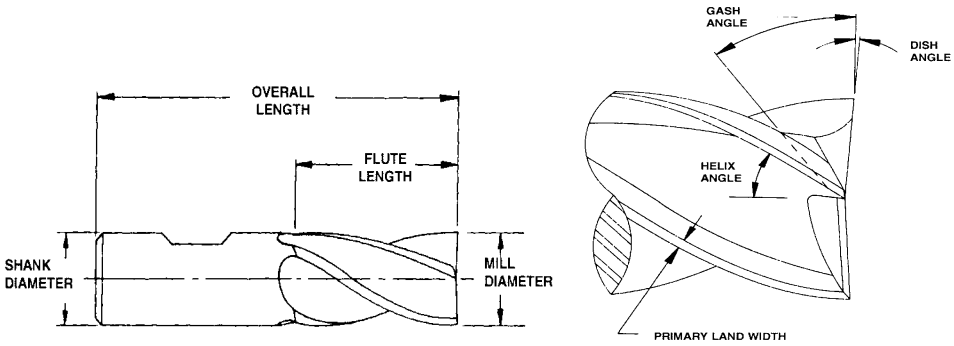

Figure 1.4: Geometric properties of the end mill

Static and dynamic deformations of cutting tool play an important role in tolerance integrity and stability in a machining process affecting part quality and productivity. Modeling is needed for prediction static and dynamic properties of cutting tool without measurement. The models can be integrated into CAD/CAM systems in order to achieve a virtual machining system where most of the effects that are observed in real machining could be simulated in advance.

1.1. Related Literature Review

Process modeling is needed for modeling structural properties of milling system components. Modeling of milling process has been the subject of many studies some of which are summarized by Smith and Tlusty (1991). The focus of these studies has mostly been on the modeling of cutting geometry and force, stability and prediction of part quality. Milling forces have been investigated using different approaches. Koenigsberger and Sabberwal (1961) developed equations for milling forces using mechanistic modeling where the cutting force coefficients which relate the chip area to tangential, radial and axial forces are calibrated through force measurements. The mechanistic approach has been widely used for the force predictions and also have been extended to predict associated machine component deflections or surface geometrical errors (Kline et al., 1982**;** Budak and Altintas, 1995). Another alternative is to use mechanics of cutting approach in determining milling force coefficients as used by Armarego et al. (1985). In this approach, an oblique cutting force model together with an orthogonal cutting database are used to predict milling force coefficients eliminating the need for milling tests as different tool and cutting geometries can be handled by the oblique model (Budak et al. 1996). Once the cutting force coefficients are known, the milling forces can be determined by integrating the forces along the cutting edges. Altintas et al. (1996, 2001) also demonstrated the application of this approach to complex milling cutter geometries. Milling forces can be used to predict tool and part deflection and form errors. (Figure 1.5)

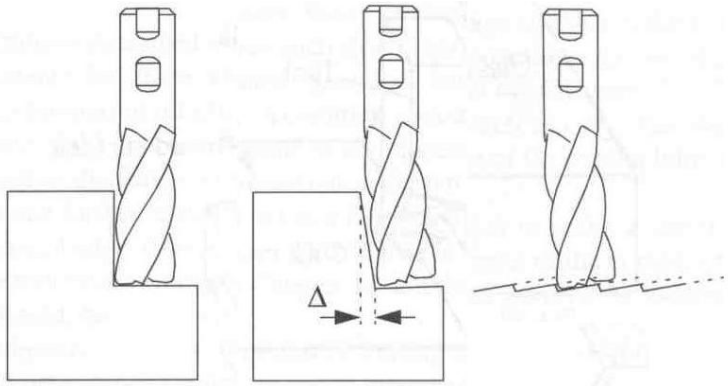

a) Ideal geometry b) Form error c) Surface roughness

Figure 1.5: Effect of tool deflection on form error and surface roughness

Another major limitation on productivity and surface quality in milling is the chatter vibrations which develop due to dynamic interactions between the cutting tool and workpiece, and result in poor surface finish and reduced tool life. Tlusty et al. (1963) and Tobias (1965) identified the most powerful source of self-excitation which is associated with the structural dynamics of the machine tool and the feedback between the subsequent cuts on the same cutting surface resulting in regeneration of waviness on the cutting surfaces, and thus modulation in the chip thickness (Koenigsberger and Tlusty, 1967). Under certain conditions the amplitude of vibrations grows and the cutting system becomes unstable. Additional operations, mostly manual, are required to clean the chatter marks left on the surface (Figure 1.6). Thus, chatter vibrations result in reduced productivity, increased cost and inconsistent product quality.

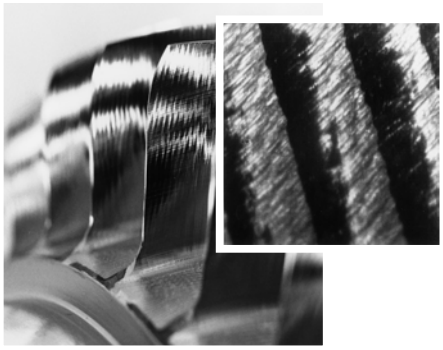

Figure 1.6: Chatter marks on the surface

CAD/CAM is the most common example of computer integration to manufacturing environment promising improved productivity, quality and flexibility. They are the most important elements for development of virtual machining systems. One significant shortcoming of CAD/CAM systems is the fact that they mostly neglect the mechanics of the process when simulating the machining cycles. Many quality and productivity problems such as excessive forces, deformations and vibrations resulting in reduced material removal rates, on the other hand, are experienced during the machining. Process models together with structural models of machining system components need to be integrated into CAD/CAM environment in order to achieve a virtual machining system where most of the effects that are observed in real machining could be simulated in advance.

Demonstrations of cutting model implementation in CAD/CAM systems have been done in several studies [Altintas and Spence, 1991, Yazar et al., 1994]. Altintas and Spence (1991), and Yazar et al. (1994) demonstrated that force models could be used to predict form errors and optimize feedrates based on simulation at the CAD/CAM stage. Weck et al. (1994) demonstrated determination of chatter free milling conditions in a commercial CAD/CAM software. Cutting force coefficients and tool dynamics were needed for these simulations, which were determined experimentally. Generation of an orthogonal cutting database for a work material as Budak et al. (1996) did reduces the amount of experiments, and thus makes implementation of force models in CAD/CAM more practical. There is a need for more practical determination of structural properties of the cutting tool for a virtual machining system. Kops et al. (1990) determined an equivalent diameter for end mill based on FEA in order to be able to use beam equations for deflection calculations, which eliminate stiffness measurements for each tool.

Static and dynamic deformations of machine tool, tool holder and cutting tool play an important role in tolerance integrity and stability in a machining process affecting part quality and productivity. Excessive static deflections may cause tolerance violations whereas chatter vibrations result in poor surface finish. Cutting force, surface finish and cutting stability models can be used to predict and overcome these problems. This would require static and dynamic data for the structures involved in a machining system (Altintas, 2000). Considering great variety of machine tool configurations, tool holder and cutting tool geometries, analysis of every case can be quite time consuming and unpractical. These data are usually obtained by testing using stiffness measurements and modal analysis (Altintas, 2000, Budak and Altintas, 1994 and Koenigsberger and Tlusty, 1967).

Recent improvements in machine and spindle designs have led to the increased use of high-speed machining (HSM) in the manufacture of discrete parts (Smith et al., 1998). It is recognized that a major practical limitation on the productivity of HSM systems is regenerative chatter. Therefore, many studies have explored methods to maximize material removal rate (MRR) during HSM, while avoiding chatter. HSM simulation, which is crucial for pre-process chatter prediction and avoidance, requires knowledge of the system

dynamics reflected at the tool point. In general, a separate set of tool point frequency response function (FRF) measurements must be performed for each tool/holder/spindle combination on a particular machining center. These measurements can prove time consuming and lead to costly machine downtime. In order to reduce measurement time and increase process efficiency receptance coupling substructure analysis (RCSA) is used to predict the tool point dynamic response. Building on early work of Duncan (1947), Bishop and Johnson (1960) and more recent work of Ewins (1986) and Ferreira and Ewins (1995). Schmitz and Donaldson (2000) and Schmitz et al. (2001) develop an analytic expression for the frequency response at the free end of the milling cutter from: 1) an analytic model of the tool; 2) an experimental measurement of the holder/spindle sub-assembly; and 3) a set of empirical connection parameters. These parameters are extracted from a single measurement of the tool/holder/spindle assembly at a known tool overhang length using nonlinear least squares estimation (Schmitz and Burn, 2003).

1.2. Scope of the Study

Due to its wide use in industry, milling system is considered. The main concern of this master thesis is the accurate knowledge the static and dynamic properties of machining system components. Generalized equations are presented which can be used for predicting the static and dynamic properties. Substructuring methods are used in predicting the total system dynamics based on component analysis. Results presented here can be integrated to a CAD/CAM environment together with process models towards development of a virtual machining system.

End milling is a commonly used process in industry for parts with dimensional and surface quality requirements. Chapter 2 gives process models (Budak, 2002) that can be used improve productivity and quality. An analytical milling force model, which is used

tool deflection calculations, is presented. The prediction of form error is demonstrated. An analytical model for prediction of chatter stability limit is presented.

Chapter 3 gives simplified equations to predict maximum tool deflection. Because of the complex end mill geometry beam approximations do not provide accurate stiffness and transfer function predictions. The moment of inertias of different end mill cross sections must be determined (Nermes et al., 2001). In static analysis, moment area method (Beer and Johnson, 1992) is used to calculate the deflection of end mill, which have two segments, one for part with flute and the other for the shank. I-DEAS (Shih, 2000) finite element analysis results for tool and tool holder is also presented in this chapter Analytical equation solutions are compared with FEA results.

Chapter 4 starts with a brief explanation segmented beam model that is used to predict tool dynamics. The solution of mode shapes and fundamental natural frequency is presented (Rao, 1995). In order to avoid complex calculations simplified equations are determined. I-DEAS finite element dynamic analysis results for tool and tool holder are given. Transfer function measurement system and modal analysis are described.

The application of Receptance Coupling Substructure Analysis (RCSA) to the analytic prediction of tool point dynamic response is described in chapter 5. The interface stiffness and damping between tool and tool holder is identified. The effects of changes in tool parameters and clamping conditions are evaluated.

In chapter 6, the analytical static and dynamic calculations are verified by experiments. Displacement of the tool is measured. Maximum surface errors due to the tool deflection are calculated and compared with experimental data (Budak and Altintas, 1994). Application of simplified segmented beam equations is demonstrated by examples.

A conclusion of the study is provided in Chapter 7 summarizing the results achieved.

CHAPTER 2

PROCESS MODELING IN MILLING

High cutting forces, tool breakage, part and tool deflections and chatter vibrations are the common reasons for reduced productivity and quality in many milling operations. Milling process can be modeled in order to overcome or reduce the effects of these limitations. In this chapter, modeling methods of force, deflection, surface error and stability are presented.

For a stable milling process, milling forces, part and tool deflections can be determined using static analysis. The force predictions can be used to determine structural deformations and form errors left on the finished surface. In the first and second section, force and structural models are described.

Another very important limitation in milling is the self-exited chatter vibrations, which cause poor surface finish and tool life resulting in reduced productivity. In the third section, mathematical models for chatter are presented.

2.1. Milling Force Modeling

Milling forces can be modeled for given cutter geometry, cutting conditions, and work material. The geometry of chip formation and milling force components is shown in Figure 2.1. (Budak, 2002**).**

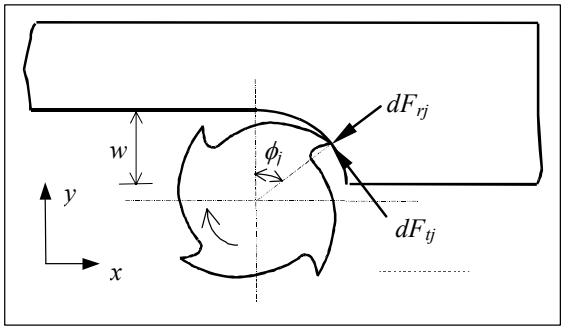

Figure 2.1: Cross sectional view of an end mill showing differential forces

Tangential (dF_t) and radial (dF_r) forces act on a differential flute element with height dz. For a point on the (j^{th}) cutting tooth, differential milling forces in the tangential (dF_t) and radial direction (dF_r) can be given as

$$\begin{aligned} dF_{t_j}(\phi,z) &= K_t h_j(\phi,z)dz \\ dF_{r_j}(\phi,z) &= K_r dF_{t_j}(\phi,z) \end{aligned} \tag{2.1}$$

where ϕ is the immersion angle measured from the positive y axis as shown in Figure 2.1. The radial (w) and axial depth of cut (a), number of teeth (N), cutter radius (R) and helix angle (β) determine what portion of a tooth is in contact with the workpiece for a given angular orientation of the cutter (ϕ). In milling the instantaneous chip thickness variation can be approximated as

$$h_j(\phi,z) = f_t \sin\phi_j(z) \tag{2.2}$$

where f_t is the feed per tooth (mm/rev-tooth) and $\phi_j(z)$ is the immersion angle for the flute (j) at axial position z.

In equation 2.1 K_t and K_r are the milling force coefficients. All milling force coefficients depend on the workpiece material and cutting tool geometry. In exponential force model, milling force coefficients K_t and K_r can be expressed as exponential functions of the average chip thickness. (Altintas, 2000) In linear force model, both cutting and edge force coefficients are assumed to be independent of the chip thickness.

$$K_t = K_T h_a^{-p}; \;\; K_r = K_R h_a^{-q} \tag{2.3}$$

where p and q are cutting force constants determined from cutting experiments at different feed rates. Average chip thickness (h_a)

$$h_a = \frac{\int_{\phi_{start}}^{\phi_{exit}} f_t \sin\phi d\phi}{\phi_{exit} - \phi_{start}} \tag{2.4}$$

In equation (2.1) the edge forces are also included in the cutting force coefficient, which is usually referred to as the exponential force model. They are separated from the cutting force coefficients in edge force or linear force model (Budak, 1994; Budak et al., 1996):

$$\begin{aligned} dF_{t_j}(\phi, z) &= \left[K_{te} + K_{tc} h_j(\phi, z) \right] dz \\ dF_{r_j}(\phi, z) &= \left[K_{re} + K_{rc} h_j(\phi, z) \right] dz \end{aligned} \tag{2.5}$$

where K_{tc} and K_{rc} are the cutting force coefficients contributed by the shearing action in tangential and radial directions, respectively and K_{te} and K_{re} are the edge constants.

Due to the helical flute, the immersion angle changes along the axial direction as

$$\phi_j(z) = \phi + (j-1)\phi_p - \frac{\tan\beta}{R} z \tag{2.6}$$

where the cutter pitch angle (or tooth spacing angle) is defined as $\phi_p=2\pi/N$. At an axial depth of cut z the lag angle is $\psi=k_\beta z$, where $k_\beta=\tan\beta/R$.

The tangential and radial forces can be resolved in the feed, x, and normal, y, directions using the transformation as follows

$$\begin{aligned} dF_{x_j} &= -dF_{t_j}\cos\phi_j - dF_{r_j}\sin\phi_j \\ dF_{y_j} &= dF_{t_j}\sin\phi_j - dF_{r_j}\cos\phi_j \end{aligned} \tag{2.7}$$

The differential cutting forces are integrated analytically along the in-cut portion of the flute j in order to obtain the total cutting force produced by the flute:

$$F_{x,y}(\phi_j(z)) = \int_{z_{jl}}^{z_{ju}} dF_{x,y}(\phi_j(z))dz \tag{2.8}$$

where $z_{jl}(\phi_j(z))$ and $z_{ju}(\phi_j(z))$ are the lower and upper axial engagement limits of the contact or the tooth (j). The integrations are carried out by noting $\phi_j(z)=\phi+(j\text{-}1)\ \phi_p-k_\beta z$, $d\phi_j(z)=-\ k_\beta dz$ (Budak and Altintas, 1995). Thus

$$\begin{aligned} F_{x_j}(\phi) &= \frac{K_t f_t R}{4\tan\beta}\left[-\cos 2\phi_j + K_r\left(2\phi_j(z)-\sin 2\phi_j(z)\right)\right]_{z_{jl}(\phi)}^{z_{ju}(\phi)} \\ F_{y_j}(\phi) &= -\frac{K_t f_t R}{4\tan\beta}\left[\left(2\phi_j(z)-\sin 2\phi_j(z)\right)+K_r\cos 2\phi_j(z)\right]_{z_{jl}(\phi)}^{z_{ju}(\phi)} \end{aligned} \tag{2.9}$$

The cutting forces contributed by all flutes are calculated and summed to obtain the total instantaneous forces on cutter at immersion ϕ:

$$F_x(\phi) = \sum_{j=1}^{N} F_{x_j}(\phi)\ ; \qquad F_y(\phi) = \sum_{j=1}^{N} F_{y_j}(\phi) \tag{2.10}$$

2.2. Tool Deflection and Form Error

In end milling, the finished workpiece surface is perpendicular to the direction of feed. If feed and normal directions are aligned with Cartesian x and y axes respectively, any deflection in the y-axis may produce a static form error. End mills can be considered as elastic cylinder beam, cantilevered to the spindle through collet end chuck. Flexible cutters deflect under the periodically varying milling forces, which are modeled in the previous section.

Generating the surface becomes complex when the end mill has helical flutes. The cutting forces are not constant but vary with the rotation of the end mill. Furthermore, the helix angle of the flutes produces additional variation on distribution of cutting forces along the z-axis. As the end mill rotates, the tip of the flute moves to immersion ϕ. Since the normal cutting force will not be zero at this instant, the elastic end mill displacement will produce a form error on the surface. Depending on the number of flutes and width of cut, there may be more than one cutting edge point in contact with the finish surface.

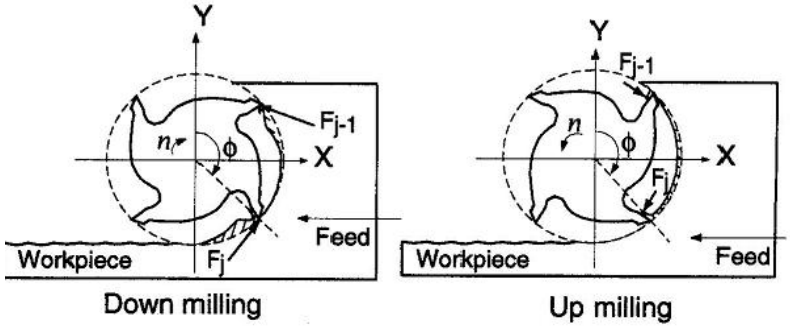

Figure 2.2: The influence of the milling mode on the surface form errors

The contact points can be calculated by equating the instantaneous immersion angle $\phi_j(z) = \phi + (j-1)\phi_p - k_\beta z$, with k_β=tanβ/R to zero in up milling and to π in down milling.

$$z = \frac{\phi + (j-1)\phi_p}{k_\beta} \text{(up milling)};\ z = \frac{\pi - (\phi + (j-1)\phi_p)}{k_\beta} \text{ (down milling)}, j=1,2..N\text{-}1 \qquad (2.11)$$

where β is the helix angle and $\phi_p=(2\pi)/N$ is the cutter pitch angle. The cutter can be divided into M number of small disk elements within the axial depth of cut (a) and it can be rotated at increments $\Delta\phi$, (i.e., $\phi=0, \Delta\phi, 2\Delta\phi, \ldots, \phi_p$) (Figure 2.3) (Altintas, 2000).

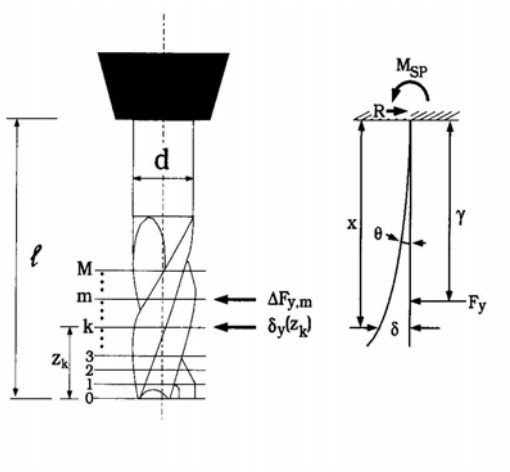

Figure 2.3: Static deformation model of an end mill

Each differential element has an axial depth of cut ($\Delta z=a/M$), and the influence of the helix angle may be neglected by selecting small elements. The differential cutting force produced by element m is given by

$$\Delta F_{y,m}(\phi) = K_t f_t \Delta z \sum_{j=0}^{N-1} [\sin\phi_j(z) - K_r \cos\phi_j(z)] \sin\phi_j \tag{2.12}$$

where K_t and K_r are cutting constants and f_t is the feed rate per tooth.

The immersion angle for the element m is $\phi_j(m)= \phi+(j-1)\ \phi_p-k_\beta.m\Delta z$. The deflection in the y direction at the contact point z_k caused by the force applied at the element m is given by the cantilever beam formulation. As

$$\delta_y(z_k,m) = \begin{cases} \dfrac{\Delta F_{y,m} v_m^2}{6EI}(3v_m - v_k), & 0 < v_k < v_m \\ \dfrac{\Delta F_{y,m} v_m^2}{6EI}(3v_k - v_m), & v_m < v_k \end{cases} \tag{2.13}$$

where E is the young modulus, I is the area of inertia of the tool and $v_k=l-z_k$, with l being the gage length of the cutter measured form the collet face. The calculation of the area moment inertia of the tool with flute will be explained in chapter 3. The total static deflection at axial contact point z_k is calculated by superposition of the deflections produced by all M elemental forces on the end mill:

$$\delta_y(z_k) = \sum_{m=1}^{M} \delta_y(z_k, m) \tag{2.14}$$

At the points where the cutting edges is contact with the finish surface, the deflection $\delta_y(z_k)$ is imprinted as a dimensional error on the workpiece.

2.3. Milling Stability

Chatter in milling has been modeled analytically by considering the regeneration in chip thickness and the machine-process interactions. Milling cutters can be considered to have two orthogonal degrees of freedom as shown in Figure 2.4. (Altintas, 2000)

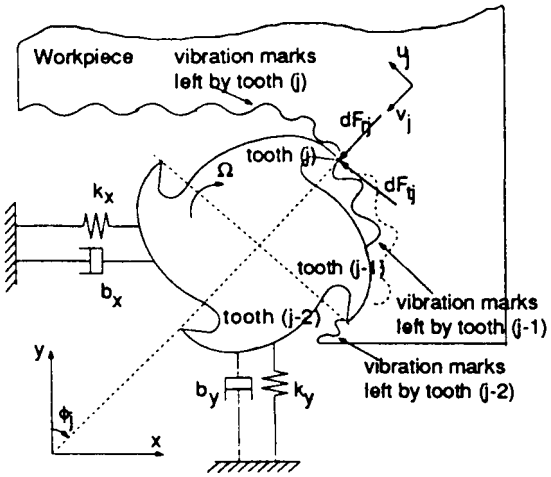

Figure 2.4: Chatter model for milling.

Milling forces excite both cutter and workpiece causing vibrations, which are imprinted on the cutting surface. Each vibrating cutting tooth removes the wavy surface left

from the previous tooth resulting in modulated chip thickness, which can be expressed as follows

$$h_j(\phi) = f_t \sin\phi_j + (v_{j_c}^o - v_{j_w}^o) - (v_{j_c} - v_{j_w}) \tag{2.15}$$

where the feed per tooth f_t represents the static part of the chip thickness, and $\phi=\Omega.t$ is the angular position of the cutter measured with respect to the first tooth and corresponding to the rotational speed Ω (rad/sec). In the equation 2.15, c and w indicate cutter and workpiece, respectively. v_j and v_j^o are the dynamic displacements due to tool and workpiece vibrations for the current and previous tooth passes, and include tool and workpiece vibrations. The static part in equation is neglected in the stability analysis. Then the dynamic chip thickness can be put in the following form

$$h_j(\phi) = [\Delta x \sin\phi_j + \Delta y \cos\phi_j] \tag{2.16}$$

where

$$\Delta x = (x_c - x_c^o) - (x_w - x_w^o)$$
$$\Delta y = (y_c - y_c^o) - (y_w - y_w^o)$$

where (x_c,y_c) and (x_w,y_w) are the dynamic displacements of the cutter and workpiece in x and y directions, respectively. Similar to the static force analysis, dynamic cutting forces can be obtained using the dynamic chip thickness as

$$\begin{Bmatrix} F_x \\ F_y \end{Bmatrix} = \frac{1}{2} a K_t \begin{bmatrix} a_{xx} & a_{xy} \\ a_{yx} & a_{yy} \end{bmatrix} \begin{Bmatrix} \Delta x \\ \Delta y \end{Bmatrix} \tag{2.17}$$

where the directional coefficients are given as:

$$\begin{aligned} a_{xx} &= -\sum_{j=1}^{N} \sin 2\phi_j + K_r(1-\cos 2\phi_j) \\ a_{xy} &= -\sum_{j=1}^{N} (1+\cos 2\phi_j) + K_r \sin 2\phi_j \\ a_{yx} &= -\sum_{j=1}^{N} -(1-\cos 2\phi_j) + K_r \sin 2\phi_j \\ a_{xx} &= -\sum_{j=1}^{N} -\sin 2\phi_j + K_r(1+\cos 2\phi_j) \end{aligned} \tag{2.18}$$

The directional coefficients, a, depend on the angular position of the cutter which makes equation (2.17) time-varying:

$$\{F(t)\} = \frac{1}{2} a K_t [A(t)] \{\Delta(t)\} \tag{2.19}$$

$[A(t)]$ is periodic at the tooth passing frequency $\omega = N\Omega$ and with corresponding period of $T = 2\pi/\omega$. In general, Fourier series expansion of the periodic term is used for the solution of the periodic systems. The higher harmonics do not affect the accuracy of the predictions, and it is sufficient to include only the average term in the Fourier series expansion of the periodic terms (Budak et al., 1994; 1998). As the directional coefficients are valid within the cutting zone between start and exit immersion angles (ϕ_{st}, ϕ_{ex}):

$$[A_0] = \frac{1}{\phi_p} \int_{\phi_{st}}^{\phi_{ex}} [A(\phi)] d\phi = \frac{N}{2\pi} \begin{bmatrix} \alpha_{xx} & \alpha_{xy} \\ \alpha_{yx} & \alpha_{yy} \end{bmatrix} \tag{2.20}$$

where

$$\begin{aligned}
\alpha_{xx} &= \frac{1}{2} \left[\cos 2\phi - 2K_r \phi + K_r \sin 2\phi \right]_{\phi_{st}}^{\phi_{ex}} \\
\alpha_{xy} &= \frac{1}{2} \left[-\sin 2\phi - 2\phi + K_r \cos 2\phi \right]_{\phi_{st}}^{\phi_{ex}} \\
\alpha_{yx} &= \frac{1}{2} \left[-\sin 2\phi + 2\phi + K_r \cos 2\phi \right]_{\phi_{st}}^{\phi_{ex}} \\
\alpha_{yy} &= \frac{1}{2} \left[-\cos 2\phi - 2K_r \phi - K_r \sin 2\phi \right]_{\phi_{st}}^{\phi_{ex}}
\end{aligned} \tag{2.21}$$

Substituting equation (2.20-21) into equation 2.19 and assuming harmonic functions for dynamic forces and vibrations, the characteristics equation is obtained as

$$\det\left[[I] + \Lambda [G_0(i\omega_c)] \right] = 0 \tag{2.22}$$

where $[I]$ is the unit matrix, and the oriented transfer function matrix is defined as:

$$
\begin{aligned}
&[G_0] = [A_0][G] \\
&[G(i\omega_c)] = [G_c(i\omega_c)] + [G_w(i\omega_c)] \\
&[G_p] = \begin{bmatrix} G_{p_{xx}} & G_{p_{xy}} \\ G_{p_{yx}} & G_{p_{yy}} \end{bmatrix} \qquad (p = c, w)
\end{aligned}
\tag{2.23}
$$

and the eigenvalue (Λ) in equation (2.22) is given as

$$
\Lambda = -\frac{N}{4\pi} K_t a \left(1 - e^{-i\omega_c T}\right) \tag{2.24}
$$

If the eigenvalue Λ is known, the stability limit can be determined from equation (2.24). Λ can easily be computed from equation (2.22) numerically. However, an analytical solution is possible if the cross transfer functions, G_{xy} and G_{yx}, are neglected in equation (2.22):

$$
\Lambda = -\frac{1}{2a_0}\left(a_1 \pm \sqrt{a_1^2 - 4a_0}\right) \tag{2.25}
$$

where

$$
\begin{aligned}
a_0 &= G_{xx}(i\omega_c) G_{yy}(i\omega_c)\left(\alpha_{xx}\alpha_{yy} - \alpha_{xy}\alpha_{yx}\right) \\
a_1 &= \alpha_{xx} G_{xx}(i\omega_c) + \alpha_{yy} G_{yy}(i\omega_c)
\end{aligned}
\tag{2.26}
$$

Since the transfer functions are complex, Λ will have complex and real parts. The axial depth of cut (a) is a real number. When $\Lambda = \Lambda_R + i\Lambda_I$ and $e^{-i\omega_c T} = \cos\omega_c T - i\sin\omega_c T$ are substituted in equation 2.24, the complex part of the equation has to vanish yielding

$$
\kappa = \frac{\Lambda_I}{\Lambda_R} = \frac{\sin\omega_c T}{1 - \cos\omega_c T} \tag{2.27}
$$

The above can be solved to obtain a relation between the chatter frequency and the spindle speed (Budak et al., 1995; 1998):

$$\omega_c T = \varepsilon + 2k\pi$$
$$\varepsilon = \pi - 2\psi \;;\; \psi = \tan^{-1}\kappa \tag{2.28}$$
$$n = \frac{60}{NT}$$

where ε is the phase difference between the inner and outer modulations, k is an integer corresponding to the number of vibration waves within a tooth period, and n is the spindle speed (rpm). After the imaginary part in equation (2.24) is vanished, the following is obtained for the stability limit (Budak and Altintas, 1995; 1998):

$$a_{\lim} = -\frac{2\pi\Lambda_R}{NK_t}\left(1+\kappa^2\right) \tag{2.29}$$

Equations (2.28-29) can be used to determine the stability limit and corresponding spindle speed. When this procedure is repeated for a range of chatter frequencies and number of vibration waves, k, the stability lobe diagram for a milling system is obtained.

2.4. Importance of the Static and Dynamic Properties of Cutting Tools

Static and dynamic properties of machine tool play an important role in a machining process. The knowledge of static and dynamic deflections of the end mill are required to predict the form errors and chatter stability limits in milling without experimental measurements.

Excessive forces, deformations and vibrations are experienced during the machining and these problems cause many quality and productivity problems. Process models together with structural models of machining system components need to be integrated into CAD/CAM environment in order to predict and compensate surface errors and determine chatter free machining condition. In a virtual machining system, most of the effects that are observed in real machining could be simulated in advance. This is very important in

CAD/CAM systems where part accuracy and the optimal stable cutting conditions can be determined before the machining process.

Therefore, force, form error and stability models can be used to improve productivity, dimensional integrity and surface finish quality in milling operations

2.5. Summary

In this chapter, milling process models are reviewed. These models can be used in optimization of milling operations. Deflection and surface generation model is used to predict form error. Stability lobes are obtained by using chatter model in order to determine suitable spindle speed. Importance of the static and dynamic properties of tool is emphasized.

CHAPTER 3

MODELING OF END MILL STATICS

Static deflection of end mills may cause tolerance violation on milled parts. These deflection need to be modeled in order to check the tolerance integrity for potential compensation of the errors. This chapter covers the static analysis of typical 2-Flute, 3-Flute and 4-Flute end mills. A cantilever beam model is used to perform the static analysis of the cutters under load. Therefore, the primary objective of the static analysis is to determine the maximum deflection at the tool tip.

In the end milling process the deflection of the cutter is an important factor affecting the accuracy of machining, with implications on the selection of cutting parameters and economics of the operation. Although the deflection affects adversely the accuracy, the flexibility of the cutter is beneficial in attenuating the overload in a sudden transient situation, as well as attenuating chatter. The end mill deflection is important to evaluate surface error.

First section of the chapter gives a brief explanation of geometric properties and analytical deflection formulas for cutters; Finite Element Analysis (FEA) results of the tool and tool holder are explained in the second section, which is followed by simplified equations for tool deflection.

3.1. Geometric Parameters and Analytical Statistical Analysis

In order to perform static analysis, models of the 2-Flute, 3-Flute and 4-Flute cutters are needed to determine the necessary geometric and loading parameters, moment of inertia and bending moments. Three models have been developed to determine the maximum deflection using cantilever method of 2-Flute, 3-Flute and 4-Flute cutters since their geometry are different. Their bending moment distributions are the same since they share same loading and boundary conditions. The loading and boundary conditions of the cantilever beam are depicted in Figure 3.1, where *D1* is the mill diameter, *D2* is the shank diameter, *L1* is the flute length, *L2* is the overall length, *F* is the point load, *I1* is the moment of inertia of the part with flute and *I2* is the moment of inertia of the part without flute. The cutting force is represented by a point force, which is an approximation. However, it should be noted that this model is used only for stiffness calculation, not for final tool deflection. Accurate surface generation models can be used (Budak and Altintas, 1994) for form errors, once the stiffness is determined.

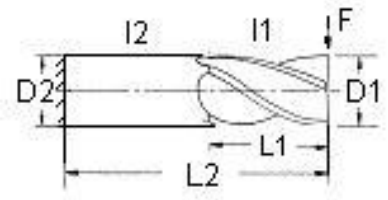

Figure 3.1: Loading and boundary conditions of the end mill

3.1.1. Moment of Inertia

In order to perform the analytic static analysis, models of the 4-Flute, 3- Flute and 2-Flute end mills are needed to determine the moment of inertias. Due to the complexity of the cutter cross-sections its axis, the calculation of the inertia is the most difficult aspect of the static analysis. The cross sections of the 3-Flute, 4- Flute and 2-Flute end mills are as shown in Figure 3.2, where f_d is the flute depth. In the case of the 3-Flute cutters, the shapes

of the regions labeled ‘1’ is bounded by the lines x=0, y=-0.5774x and arcs. The region labeled ‘2’ is bounded by the lines x=0, y=0.5774x and an arc. Lastly, the region labeled ‘3’ is bounded by the lines y=0.5774x, y=-0.5774x and an arc. Regions labeled ‘1’, ‘2’, ‘3’ and ‘4’ in the case of the 4-Flute cutters, are bounded by arcs and the lines x=0 and y=0. Regions labeled ‘1’ or ‘2’ in the cross section of the 2-Flute cutter, are bounded by the line y=0. Based on the equations bounding each region, the inertia can be derived. The derivations of the moment of inertia of the 3-Flute, 4- Flute and 2-Flute cutters are provided in Sections 3.1.1.1, 3.1.1.2 and 3.1.1.3. The flute depth, f_d, is in general different for different end mill generation.

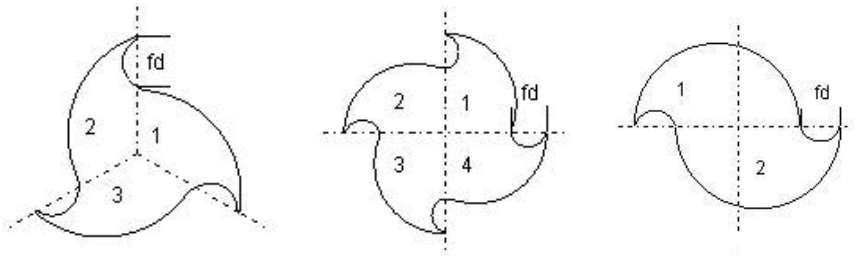

Figure 3.2: Cross-sections of the 3-Flute, 4-Flute and 2-Flute end mills

3.1.1.1. 3-Flute Cutters

In order to obtain the inertia of the cross section, inertia of region 1 is first derived and the inertia of regions 2 and 3 are obtained by transforming the inertia matrix of region 1. The total inertia of cross section is then obtained by summing the inertia of regions 1,2 and 3.

Using tensor analysis, the inertia of region 2 of a 3-Flute cutter can be obtained by transforming the inertia matrix of region 1, I_1, by 120 degrees as:

$$I_2 = T\ I_1\ T^T \tag{3.1}$$

where the inertia matrices I_1, I_2 and the transformation matrix T are defined as

$$I_1 = \begin{pmatrix} I_{xx,1} & -I_{xy,1} \\ -I_{xy,1} & I_{yy,1} \end{pmatrix}$$
$$I_2 = \begin{pmatrix} I_{xx,2} & I_{xy,2} \\ I_{xy,2} & I_{yy,2} \end{pmatrix} \tag{3.2}$$
$$T = \begin{pmatrix} \cos(\frac{2\pi}{3}) & -\sin(\frac{2\pi}{3}) \\ \sin(\frac{2\pi}{3}) & \cos(\frac{2\pi}{3}) \end{pmatrix}$$

Similarly, the inertia of region 3 can be found by transforming the inertia of region 1 by 240 degrees. That is

$$I_3 = T\ I_1\ T^T \tag{3.3}$$

where the transformation matrix T in this case is defined as

$$T = \begin{pmatrix} \cos(\frac{4\pi}{3}) & -\sin(\frac{4\pi}{3}) \\ \sin(\frac{4\pi}{3}) & \cos(\frac{4\pi}{3}) \end{pmatrix} \tag{3.4}$$

Then, the total inertia of the 3-Flute cutter can be calculated as

$$I_{xx3-flute,TOTAL} = I_{yy3-flute,TOTAL} = 1.5I_{xx,1} + 1.5I_{yy,1} \tag{3.5}$$

The cross section of the region 1 of the 3-Flute cutter is drawn as shown in Figure 3.3

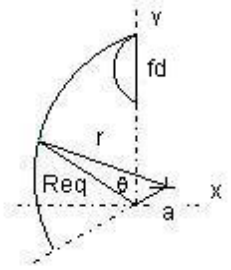

Figure 3.3: Region 1 of 4-Flute end mill

The inertia of region 1 is derived by, first computing the equivalent radius R_{eq} of the arc respect to x- and y-axes by using the cosine law, in terms of the radius r of the arc, position of the center of the arc (a) and θ. (Nermes et al., 2001)

$$R_{eq3-flute}(\theta) = a.\cos(\theta + \frac{\pi}{3}) + \sqrt{(r^2 - a^2) + a^2.\cos^2(\theta + \frac{\pi}{3})} \qquad 0<\theta \le \frac{2\pi}{3} \tag{3.6}$$

The moment of inertia about x-axis and y-axis are given as

$$\begin{aligned} I_{xx,1} &= \int_0^{2\pi/3} \int_0^{R_{eq}(\theta)} \rho^3 \sin^2(\theta) d\rho d\theta - \left[\frac{1}{8}\pi(\frac{fd}{2})^4 + \frac{\pi(\frac{fd}{2})^2}{2}.(\sqrt{r^2 + a^2} - \frac{fd}{2})^2 \right] \\ I_{yy,1} &= \int_0^{2\pi/3} \int_0^{R_{eq}(\theta)} \rho^3 \cos^2(\theta) d\rho d\theta - \left[\frac{1}{8}\pi(\frac{fd}{2})^4 \right] \end{aligned} \tag{3.7}$$

Performing the first integral with respect to ρ and rearranging, equation. (3.7) becomes

$$\begin{aligned} I_{xx,1} &= \frac{1}{4} \int_0^{2\pi/3} {R_{eq}}^4 \sin^2(\theta) d\theta - \left[\frac{1}{8}\pi(\frac{fd}{2})^4 + \frac{\pi(\frac{fd}{2})^2}{2}.(\sqrt{r^2 + a^2} - \frac{fd}{2})^2 \right] \\ I_{yy,1} &= \frac{1}{4} \int_0^{2\pi/3} {R_{eq}}^4 \cos^2(\theta) d\theta - \left[\frac{1}{8}\pi(\frac{fd}{2})^4 \right] \end{aligned} \tag{3.8}$$

Substituting $R_{eq3\text{-}flute}$ (3.6) into integrals and integrating we get the moment of inertia about x-axis and y-axis for region 1 of the 3-Flute end mill. $I_{xx,1}$ and $I_{yy,1}$ are used to evaluate the total moment of the inertia (3.5).

3.1.1.2. 4-Flute Cutters

In the case of the 4-Flute cutters, the cross section of the region 1 is drawn as shown in Figure 3.4. The regions 1,2,3 and 4 are symmetrical, therefore the inertia of only one region is necessary to compute and the inertias of the other regions are deduced. For instance, it can be shown that the inertia of region 1 about the x-axis, $I_{xx,1}$, is equal to the inertia of region 2 about the y-axis, $I_{yy,2}$. The total inertia as function of the inertia of the region 1 is found as

$$I_{xx4-flute,TOTAL} = I_{yy4-flute,TOTAL} = 2I_{xx,1} + 2I_{yy,1} \tag{3.9}$$

The inertia of region 1 is derived by, computing the equivalent radius R_{eq} of the arc with respect to x- and y-axes by using the cosine law in terms of r, a and θ.

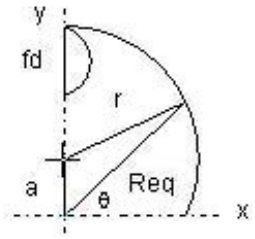

Figure 3.4: Region 1 of 4-Flute end mill

The equivalent radius formula for region 1 of 4-Flute end mill with respect to x- and y-axes is given as follows

$$R_{eq4-flute}(\theta) = a.\sin(\theta) + \sqrt{(r^2 - a^2) + a^2.\sin^2(\theta)} \qquad 0<\theta \le \frac{\pi}{2} \tag{3.10}$$

The moment of inertia about x-axis and y-axis are found as

$$\begin{aligned} I_{xx,1} &= \frac{1}{4}\int_0^{\pi/2} {R_{eq}}^4 \sin^2(\theta)d\theta - \left[\frac{1}{8}\pi(\frac{fd}{2})^4 + \frac{\pi(\frac{fd}{2})^2}{2}.(r + a - \frac{fd}{2})^2\right] \\ I_{yy,1} &= \frac{1}{4}\int_0^{\pi/2} {R_{eq}}^4 \cos^2(\theta)d\theta - \left[\frac{1}{8}\pi(\frac{fd}{2})^4\right] \end{aligned} \tag{3.11}$$

Substituting $R_{e4\text{-}flute}$ (3.10) into integrals and integrating we obtain $I_{xx,1}$ and $I_{yy,1}$ and they are used to evaluate the total moment of the inertia (3.9).

3.1.1.3. 2-Flute Cutters

In the case of the 2-Flute cutters, the cross section of the region 1 is drawn as shown in Figure 3.5. The cross section of the 2-Flute cutter is not symmetric with respect to x and y-axes, so the total moment of inertia I_{xx} and I_{yy} are different. After transforming and summing, the total moment of inertia of the 2-Flute end mill is found as

$$I_{xx2-flute,TOTAL} = 2I_{xx,1},\ I_{yy2-flute,TOTAL} = 2I_{yy,1} \tag{3.12}$$

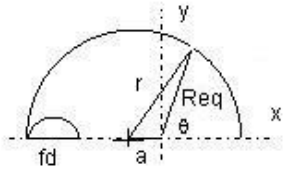

Figure 3.5: Region 1 of 2-Flute end mill

The inertia of region 1 of the 2-Flute cutter is derived by computing the equivalent radius R_{eq} by using the cosine law in terms of r, a and θ.

$$R_{eq2-flute}(\theta) = -a.\cos(\theta) + \sqrt{(r^2 - a^2) + a^2.\cos^2(\theta)} \qquad 0<\theta<\pi \tag{3.13}$$

The moment of inertia about x- and y-axes are given as

$$\begin{aligned} I_{xx,1} &= \frac{1}{4}\int_0^{\pi} {R_{eq}}^4 \sin^2(\theta)d\theta - \left[\frac{1}{8}\pi(\frac{fd}{2})^4\right] \\ I_{yy,1} &= \frac{1}{4}\int_0^{\pi/2} {R_{eq}}^4 \cos^2(\theta)d\theta - \left[\frac{1}{8}\pi(\frac{fd}{2})^4 + \frac{\pi(\frac{fd}{2})^2}{2}.(r-\frac{fd}{2})^2\right] \end{aligned} \tag{3.14}$$

We obtain $I_{xx,1}$ and $I_{yy,1}$ by substituting $R_{eq2\text{-}flute}$ (3.13) into integrals and integrating. They are used to evaluate the total moment of the inertia (3.12).

3.1.2. Maximum Deflection

Knowing the moment of inertia of the 4-Flute, 3- Flute and 2-Flute end mills, the deflection along the length of cutters can be calculated for given material properties (*E*, elastic modulus) and force (*F*). Based on the loading conditions, the deflection along the beam is determined by using the moment area theorems. For example, Figure 3.6 shows the variation along two parts of a beam of the quantity *M/EI*, obtained by dividing the bending moment *M* by the flexural rigidity *EI* (Elastic Modulus* Moment of Inertia).

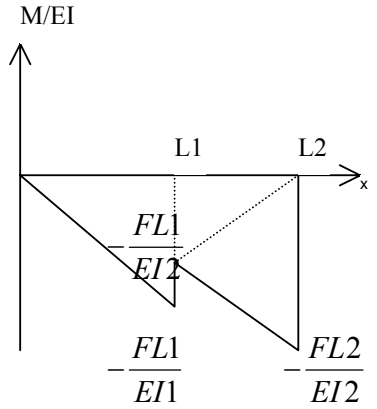

Figure 3.6: Bending moment (ME/I) diagram of the end mill

The product of the area, which refers to the area under the *M/EI* diagram, and the distance from its centroid to origin gives the maximum deflection at the end point. From Figure 3.6 using moment area method we can define y_{max} for the end point (Beer and Johnston, 1992).

$$y_{\max} = \frac{FL1^3}{3EI1} + \frac{1}{6}\frac{FL1(L2-L1)(L2+2L1)}{EI2} + \frac{1}{6}\frac{FL2(L2-L1)(2L2+L1)}{EI2} \tag{3.15}$$

3.2. Modeling and FEA Analysis

For parametric, geometric solid modeling and Finite Element Modeling (FEM) several software, such as CATIA, Pro/Engineer and I-DEAS, can be used. For this research, I-DEAS is used for geometric modeling and FEM.

3.2.1. Tool

3.2.1.1. Parametric Geometric Modeling

For geometric modeling of 4-Flute, 3-Flute and 2-Flute, helical end mills, I-DEAS is a powerful parametric design tool. I-DEAS is a Computer Aided Engineering package used to create three-dimensional (3D) solid models of parts. I-DEAS is a parametric solid modeling system that makes design changes easy to oerform. Parametric means that the shape of the part is driven by its feature dimensions. Feature dimensions can be redefined at anytime. Many 3D solid models were prepared for end mills with different flute diameter, shank diameter, flute length, overall length and flute number.

3.2.1.2. Finite Element Modeling (FEM) and Analysis (FEA)

Finite element modeling and analysis are performed on I-DEAS FE package (Shih, 2000). End mills are made from high-speed steel (HSS) and carbide that have the following properties necessary to calculate the maximum deflection.

Material	Modulus of Elasticity (GPa)	Poisson's Ratio	Density (kg/m^3)
HSS	200	0.3	8600
Carbide	605	0.3	12500

Table 3.1: Mechanical properties of the tool materials

The 4-Flute, 3-Flute and 2-Flute end mills are meshed with solid linear tetrahedral elements. The end mill is split into two segments: one which represents the shank with one length of elements and an other which represents the part including Flute and cutting edges with a second length of elements. This is to reduce the total number of elements suitable for FE analysis.

The end mill is constrained at the end of the shank where it is gripped by the tool holder. The displacement is constrained at that point in all directions. This is actually a simple cantilever beam clamped at one end and free at the other end. The force is applied at the free end. Figure 3.7 illustrates an example of the meshed 3-Flute end mill including boundary conditions.

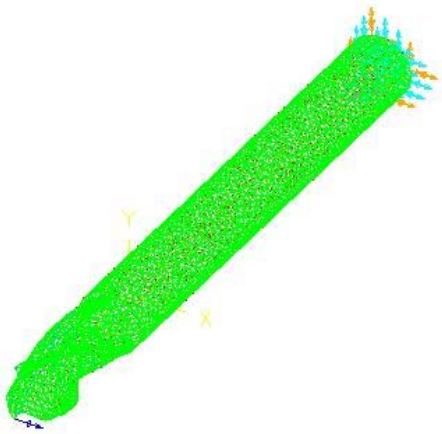

Figure3.7: Meshing and boundary conditions example

Finite Element Analysis (FEA) is applied to great variety of tool geometries and two different tool materials in I-DEAS. An example deflection of an end mill is shown in Figure 3.8. Some of the deflection values found by analytic equations and I-DEAS are shown in Table 3.2. Approximately sixty tools were tested.

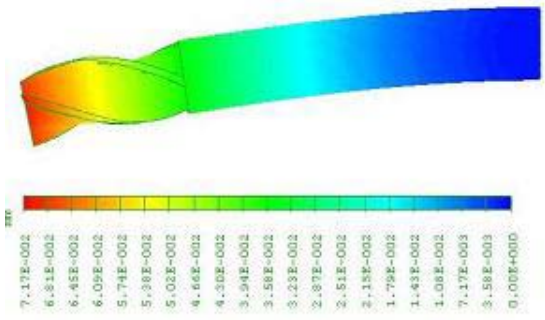

Figure 3.8: Example tool deflection

Flute	Material	D1 (mm)	D2 (mm)	L1 (mm)	L2 (mm)	y_Analytic (mm) Force=50 N	y_I-DEAS (mm) Force=50 N	Difference (%)
4	HSS	6	6	13	57	0.248844	0.251768	1.16
3	HSS	6	6	13	57	0.245466	0.250252	1.91
2	HSS	6	6	13	57	0.244309	0.249888	1.23
4	HSS	10	10	22	72	0.067320	0.069073	2.54
3	HSS	10	10	22	72	0.065174	0.067203	3.02
2	HSS	10	10	22	72	0.064452	0.066813	3.53
4	HSS	10	13	22	72	0.027316	0.028412	3.86
3	HSS	10	13	22	72	0.025169	0.026517	5.08
2	HSS	10	13	22	72	0.024448	0.026007	5.99
4	HSS	10	10	26	72	0.069894	0.071800	2.65
3	HSS	10	10	26	72	0.066350	0.068580	3.25
2	HSS	10	10	26	72	0.065160	0.0676546	3.69
4	HSS	16	19	32	92	0.012426	0.013230	6.08
3	HSS	16	19	32	92	0.011415	0.012325	7.38
2	HSS	16	19	32	92	0.010901	0.011842	7.94
4	Carbide	10	10	22	72	0.022255	0.022832	2.54
3	Carbide	10	10	22	72	0.021545	0.022216	3.02
2	Carbide	10	10	22	72	0.021307	0.022087	3.53
4	Carbide	16	16	32	92	0.007281	0.007580	3.94
3	Carbide	16	16	32	92	0.006950	0.007315	4.99
2	Carbide	16	16	32	92	0.006777	0.007163	5.38
4	Carbide	20	20	38	104	0.004368	0.004630	5.66
3	Carbide	20	20	38	104	0.004138	0.004463	7.27
2	Carbide	20	20	38	104	0.004062	0.004409	7.86

Table 3.2: Results of the analytic equations and I-DEAS analysis

3.2.1.3. Simplified Equations for Tool Deflection

Modeling and FEA can be impractical and time consuming for each tool configuration in a virtual machining environment. Therefore, simplified equations are created to predict deflections of tools for given geometric parameters and material properties (elastic modulus and density). The static characteristics of end mills can be easily determined by these analytical expressions. After the comparison of analytical and FEA results, the corrected deflection equations are obtained by using MINITAB software. These equations has the following form:

$$Y = C.Y^{N}_{analytic}$$

$$C = \begin{cases} 0.984 & \text{for 4-Flute} \\ 0.985 & \text{for 3-Flute} \\ 0.983 & \text{for 2-Flute} \end{cases} \qquad (3.16)$$

$$N = \begin{cases} 0.983 & \text{for 4-Flute} \\ 0.981 & \text{for 3-Flute} \\ 0.980 & \text{for 2-Flute} \end{cases}$$

where $Y_{analytic}$ is in mm. The error in this approximation is less than % 1.

In the analytical deformation equations, the evaluation of the integral formulas is very complex. In an attempt to further simplify the deflection calculation, the following analysis is performed. The maximum deflection could be determined using

$$deflection_{\max} = C.\frac{F}{E}\left[\frac{L1^3}{D1^4} + \frac{(L2^3 - L1^3)}{D2^4}\right]^N$$

$$C = \begin{cases} 9.05 & \text{for 4-Flute} \\ 8.30 & \text{for 3-Flute} \\ 7.93 & \text{for 2-Flute} \end{cases} \qquad (3.17)$$

$$N = \begin{cases} 0.950 & \text{for 4-Flute} \\ 0.965 & \text{for 3-Flute} \\ 0.974 & \text{for 2-Flute} \end{cases}$$

where F(N) is the applied force and E (MPa) is the modulus of elasticity of the tool material. The geometric properties of the end mill are in mm. The error in this approximation is less than % 5.

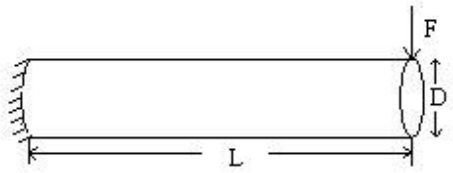

Figure 3.9: Boundary and loading conditions of the cylinder

If the shape of the end mill is assumed to be a cylinder, the stiffness of the tool will be very different from the stiffness obtained from simplified equations (Table 3.3). Figure 3.9 shows boundary and loading conditions of a cylinder. The stiffness of the cylinder is calculated by using cantilever beam method. (Beer and Johnston, 1992)

$$y_{\max} = \frac{FL^3}{3EI} = \frac{FL^3}{3E\dfrac{\pi D^4}{64}} \rightarrow k = \frac{F}{y_{\max}} = \frac{3E\pi D^4}{64L^3} \tag{3.18}$$

where k is the stiffness (N/mm). Diameter (D) and length (L) of the cylinder are in mm and elastic modulus (E) is in MPa (N/mm^2)

Flute	Material	D1 (mm)	D2 (mm)	L1 (mm)	L2 (mm)	k_equation (N/mm)	k_cylinder (N/mm)
4	HSS	6	6	13	57	201	**206**
3	HSS	6	6	13	57	204	
2	HSS	6	6	13	57	205	
4	HSS	10	10	22	72	743	**789**
3	HSS	10	10	22	72	767	
2	HSS	10	10	22	72	776	
4	Carbide	10	10	22	72	2246	**2387**
3	Carbide	10	10	22	72	2321	
2	Carbide	10	10	22	72	2347	
4	Carbide	16	16	32	92	6867	**7498**
3	Carbide	16	16	32	92	7194	
2	Carbide	16	16	32	92	7378	

Table 3.3: Comparison of the stiffness values obtained from simplified equations and cylinder model

3.2.2. Tool Holder

The static characteristics of HSK (HSK-40, HSK-50 and HSK-63) and CAT (CAT-40 and CAT-50) tool holders were analyzed in I-DEAS. The material properties for tool holders are summarized in Table 3.4 (Aoyama and Inasaki, 2001). Examples of the finite element model used for HSK and CAT tool holders are shown in Figure 3.10.

Modulus of Elasticity (GPa)	Poisson's Ratio	Density (kg/m^3)
206	0.3	7860

Table 3.4: Mechanical Properties of the Tool Holder Material

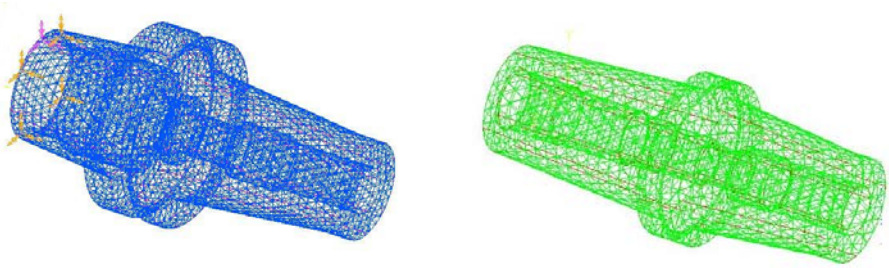

Figure 3.10: Example of FEM model for HSK and CAT tool holders

An example of deformation of the HSK type tool holder is shown in Figure 3.11. The displacement of tool holders and stiffness values are shown in Table 3.5.

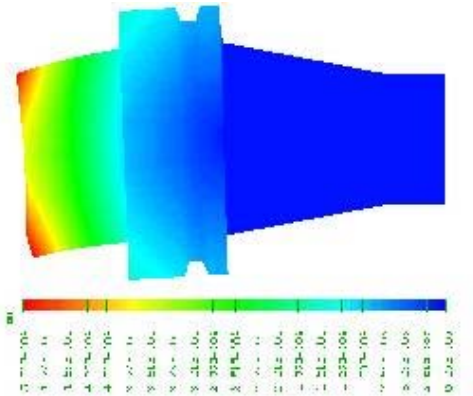

Figure 3.11: Example of deflection of a tool holder

Tool Holder Type	Max Displacement (μm) Force=200 N	Stiffness (kN/mm)
HSK-A40	1.38	24.60
HSK-A50	3.14	63.69
HSK-A63	9.02	22.17
CAT-40	3.53	56.66
CAT-50	4.26	46.95

Table 3.5: Results of I-DEAS analysis of the tool holders

It can be concluded from Table 3.5 that the stiffness depends on the type of the tool holder.

3.3. Summary

In this chapter, geometric properties and material characteristics of tool and tool holder are explained. Models for end mill static deformations, which can be used for deflection calculations and surface form error, are presented. Generalized equations are developed to predictions stiffness for different tool geometry without measurement. The static characteristics of tool and tool holder are obtained using FEA analysis. FEA results are compared with analytical equation results.

CHAPTER 4

MODELING OF END MILL DYNAMICS

In this chapter, the dynamic analysis of milling tool and tool holder is presented. Dynamic properties play an important role in stability of machining process affecting part quality and productivity. Accurate knowledge of the machine dynamics is required for predicting dimensional accuracy. Frequency response function (FRF) measurements need to be performed to identify the dynamics of the systems experimentally. This can be very time consuming considering the number of tool-tool holder combinations in a production facility.

In the first section, a method for modeling dynamics of milling tool is presented. Some practical equations are developed to predict the dynamic properties of tools. Dynamic analysis of different geometry and material of the tool and tool holder, which are carried out by Finite Element Analysis (FEA) in I-DEAS, are given in the second section. Considering great variety of cutting tool geometries, application of FEA to every case can be quite time consuming and unpractical. The results obtained from FEA and analytic dynamic equations are compared in the third section.

In the last section, the transfer function measurement and modal analysis are explained. The analytical FRF prediction method is compared with the results obtained from experiments.

4.1. Dynamic Analysis of the Tool

4.1.1. Segmented Beam Model for Tool Dynamics

Dynamic analysis is used to determine mode shapes and natural frequencies of the cutting tool structures. A modeling method for transverse vibrations of an end mill is developed. End mill is a segmented beam, one segment for the part with flute and the other segment for the shank. The beam model with two different geometric segments is shown in Figure 4.1. Dynamic analysis of segmented beam has been carried as it was not available in the vibration literature.

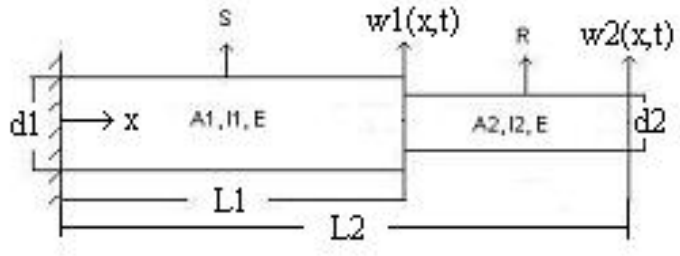

Figure 4.1: The geometry of the beam with two different geometric segments

I1, *I2* and *A1*, *A2* are the moment of inertias and the areas of the segments, respectively. *R (x)* and *S (y)* are the mode shapes, and *w1 (x, t)*, and *w2 (x, t)* are the displacement functions.

For a slender beam with two different geometric segments, the associated displacement functions *w1 (x, t)*, and *w2 (x, t)* can be written in the following form;

$$\begin{aligned} w1(x,t) &= S(x).e^{i\omega t} \quad , 0 \le x \le L1 \\ w2(x,t) &= R(x).e^{i\omega t} \quad , L1 \le x \le L2 \end{aligned} \tag{4.1}$$

The governing equations of motion, neglecting the rotational inertia and shear formation, can be converted into the well-known Euler-Bernoulli equations (Chaudhari and Maiti, 2000):

$$\begin{aligned} EI1\frac{d^4S}{dx^4} - \rho A1\omega^2 S = 0 \quad , 0 \le x \le L1 \\ EI2\frac{d^4R}{dx^4} - \rho A2\omega^2 R = 0 \quad , L1 \le x \le L2 \end{aligned} \tag{4.2}$$

where E is the modulus of elasticity and ρ is the density. The solution of equation (4.2) can be expressed as (Rao, 1995)

$$\begin{aligned} R(x) &= A1.\cosh(\beta x) + A2.\sinh(\beta x) + A3.\cos(\beta x) + A4.\sin(\beta x) \\ S(x) &= A5.\cosh(\alpha x) + A6.\sinh(\alpha x) + A7.\cos(\alpha x) + A8.\sin(\alpha x) \end{aligned} \tag{4.3}$$

where A1, A2, A3, A4, A5, A6, A7 and A8 are arbitrary constants. It is necessary to accompany the general solutions with the boundary conditions. The boundary conditions are as follows. At $x=L2$ (i.e. at the free end), bending moment and shear force must vanish:

$$\begin{aligned} &EI2\frac{d^2R(L2)}{dx^2} = 0 \rightarrow \frac{d^2R(L2)}{dx^2} = 0 \\ &A1\cosh(\beta L2) + A2\sinh(\beta L2) - A3\cos(\beta L2) - A4\sin(\beta L2) = 0 \end{aligned} \tag{4.4}$$

$$\begin{aligned} &\frac{d}{dx}EI2\left(\frac{d^2R(0)}{dx^2}\right) = 0 \rightarrow \frac{d^3R(0)}{dx^3} = 0 \\ &A1\sinh(\beta L2) + A2\cosh(\beta L2) + A3\sin(\beta L2) - A4\cos(\beta L2) = 0 \end{aligned} \tag{4.5}$$

At $x=L1$ the continuity equations for displacement, slope, moment and shear force are as follows:

$$\begin{aligned} &R(L1) = S(L1) \\ &A1\cosh(\beta L1) + A2\sinh(\beta L1) + A3\cos(\beta L1) + A4\sin(\beta L1) - \\ &A5\cosh(\alpha L1) - A6\sinh(\alpha L1) - A7\cos(\alpha L1) - A4\sin(\alpha L1) = 0 \end{aligned} \tag{4.6}$$

$$\begin{aligned} &\frac{dR(L1)}{dx} = \frac{dS(L1)}{dx} \\ &A1\sinh(\beta L1) + A2\cosh(\beta L1) - A3\sin(\beta L1) + A4\cos(\beta L1) - \\ &\frac{\alpha}{\beta}A5\sinh(\alpha L1) - \frac{\alpha}{\beta}A6\cosh(\alpha L1) + \frac{\alpha}{\beta}A7\sin(\alpha L1) - \frac{\alpha}{\beta}A8\cos(\alpha L1) = 0 \end{aligned} \tag{4.7}$$

$$\begin{aligned} &\frac{d^2R(L1)}{dx^2} = \frac{d^2S(L1)}{dx^2} \\ &A1\cosh(\beta L1) + A2\sinh(\beta L1) - A3\cos(\beta L1) - A4\sin(\beta L1) - \\ &\left(\frac{\alpha}{\beta}\right)^2 A5\cosh(\alpha L1) - \left(\frac{\alpha}{\beta}\right)^2 A6\sinh(\alpha L1) + \left(\frac{\alpha}{\beta}\right)^2 A7\cos(\alpha L1) + \left(\frac{\alpha}{\beta}\right)^2 A8\sin(\alpha L1) = 0 \end{aligned} \tag{4.8}$$

$$\frac{d^3R(L1)}{dx^3} = \frac{d^3S(0)}{dy^3}$$

$$A1\sinh(\beta L1) + A2\cosh(\beta L1) + A3\sin(\beta L1) - A4\cos(\beta L1) - \left(\frac{\alpha}{\beta}\right)^3 A5\sinh(\alpha L1) - \left(\frac{\alpha}{\beta}\right)^3 A6\cosh(\alpha L1) - \left(\frac{\alpha}{\beta}\right)^3 A7\sin(\alpha L1) + \left(\frac{\alpha}{\beta}\right)^3 A8\cos(\alpha L1) = 0 \tag{4.9}$$

At *x=0* (i.e. at the fixed end) displacement and slope are zero:

$$S(0) = 0$$
$$A5 + A7 = 0 \tag{4.10}$$

$$\frac{dS(0)}{dx} = 0$$
$$A6 + A8 = 0 \tag{4.11}$$

These 8 conditions defined by equations (4.4 - 4.11) are sufficient to solve for the 8 arbitrary constants. The equations involving these constants can be written in the following form

$$[C]\{A\} = 0 \tag{4.12}$$

where A_j is the vector of the 8 arbitrary constants and the coefficient matrix [C] is of dimension (8 x 8), and is given by

$$[C] = \begin{bmatrix}
\cosh(\beta L2) & \sinh(\beta L2) & -\cos(\beta L2) & -\sin(\beta L2) & 0 & 0 & 0 & 0 \\
\sinh(\beta L2) & \cosh(\beta L2) & \sin(\beta L2) & -\cos(\beta L2) & 0 & 0 & 0 & 0 \\
\cosh(\beta L1) & \sinh(\beta L1) & \cos(\beta L1) & \sin(\beta L1) & -\cosh(\alpha L1) & -\sinh(\alpha L1) & -\cos(\alpha L1) & -\sin(\alpha L1) \\
\sinh(\beta L1) & \cosh(\beta L1) & -\sin(\beta L1) & \cos(\beta L1) & \frac{-\alpha}{\beta}\sinh(\alpha L1) & \frac{-\alpha}{\beta}\cosh(\alpha L1) & \frac{\alpha}{\beta}\sin(\alpha L1) & \frac{-\alpha}{\beta}\cos(\alpha L1) \\
\cosh(\beta L1) & \sinh(\beta L1) & -\cos(\beta L1) & -\sin(\beta L1) & \frac{-\alpha^2}{\beta^2}\cosh(\alpha L1) & \frac{-\alpha^2}{\beta^2}\sinh(\alpha L1) & \frac{\alpha^2}{\beta^2}\cos(\alpha L1) & \frac{\alpha^2}{\beta^2}\sin(\alpha L1) \\
\sinh(\beta L1) & \cosh(\beta L1) & \sin(\beta L1) & -\cos(\beta L1) & \frac{-\alpha^3}{\beta^3}\sinh(\alpha L1) & \frac{-\alpha^3}{\beta^3}\cosh(\alpha L1) & \frac{-\alpha^3}{\beta^3}\sin(\alpha L1) & \frac{\alpha^3}{\beta^3}\cos(\alpha L1) \\
0 & 0 & 0 & 0 & 1 & 0 & 1 & 0 \\
0 & 0 & 0 & 0 & 0 & 1 & 0 & 1
\end{bmatrix} \tag{4.13}$$

The characteristic equation is determined when determinant of the coefficient matrix C (4.13) is equal to zero. In order to write of the characteristic equation with one unknown, the ratio between β and α values is calculated by using the frequency equation, which is derived from equation 4.2.

$$\frac{d^4S}{dx^4}-\frac{\rho A1}{EI1}\omega^2 S=0\rightarrow\ \frac{d^4S}{dx^4}-\alpha^4\omega^2 S=0\rightarrow\omega=\alpha^2\sqrt{\frac{EI1}{\rho A1}}$$
$$\frac{d^4R}{dx^4}-\frac{\rho A2}{EI2}\omega^2 R=0\rightarrow\frac{d^4R}{dx^4}-\beta^4\omega^2 R=0\rightarrow\omega=\beta^2\sqrt{\frac{EI2}{\rho A2}} \qquad (4.14)$$
$$\omega=\alpha^2\sqrt{\frac{EI1}{\rho A1}}=\beta^2\sqrt{\frac{EI2}{\rho A2}}\rightarrow\frac{\beta^2}{\alpha^2}=\sqrt{\frac{I2A1}{A2I1}}\rightarrow\frac{\beta}{\alpha}=\sqrt{\frac{d2}{d1}}$$

The simple form of matrix (4.13) is obtained by using $\frac{L1}{L2}$ (l) and $\sqrt{\frac{d2}{d1}}$ (d) ratios. There is only one unknown, x ($\beta L2$) in this form.

$$[C]=\begin{bmatrix}
\cosh(x) & \sinh(x) & -\cos(x) & -\sin(x) & 0 & 0 & 0 & 0\\
\sinh(x) & \cosh(x) & \sin(x) & -\cos(x) & 0 & 0 & 0 & 0\\
\cosh(xl) & \sinh(xl) & \cos(xl) & \sin(xl) & -\cosh(x\frac{l}{d}) & -\sinh(x\frac{l}{d}) & -\cos(x\frac{l}{d}) & -\sin(x\frac{l}{d})\\
\sinh(xl) & \cosh(xl) & -\sin(xl) & \cos(xl) & \frac{-1}{d}\sinh(x\frac{l}{d}) & \frac{-1}{d}\cosh(x\frac{l}{d}) & \frac{1}{d}\sin(x\frac{l}{d}) & \frac{-1}{d}\cos(x\frac{l}{d})\\
\cosh(xl) & \sinh(xl) & -\cos(xl) & -\sin(xl) & \frac{-1}{d^2}\cosh(x\frac{l}{d}) & \frac{-1}{d^2}\sinh(x\frac{l}{d}) & \frac{1}{d^2}\cos(x\frac{l}{d}) & \frac{1}{d^2}\sin(x\frac{l}{d})\\
\sinh(xl) & \cosh(xl) & \sin(xl) & -\cos(xl) & \frac{-1}{d^3}\sinh(x\frac{l}{d}) & \frac{-1}{d^3}\cosh(x\frac{l}{d}) & \frac{-1}{d^3}\sin(x\frac{l}{d}) & \frac{1}{d^3}\cos(x\frac{l}{d})\\
0 & 0 & 0 & 0 & 1 & 0 & 1 & 0\\
0 & 0 & 0 & 0 & 0 & 1 & 0 & 1
\end{bmatrix} \qquad (4.15)$$

βL2 or αL1 values are computed from characteristic equation, i.e. determinant of the coefficient matrix C (4.15) for different modes. For any beam, there will be an infinite number of normal modes with one natural frequency associated with each normal mode. The natural frequencies of segmented beam

$$\omega = (\alpha L1)^2 \sqrt{\frac{EI1}{\rho A1 L1^4}} \quad \text{or} \quad \omega = (\beta L2)^2 \sqrt{\frac{EI2}{\rho A2 L2^4}} \tag{4.16}$$

After determining the coefficient matrix *C*, arbitrary constants vector *A* can be computed from equation (4.12). The mode shapes *R (x)* and *S (y)* (equation 4.3) according to the frequencies are obtained by using *A1*, *A2*, *A3*, *A4*, *A5*, *A6*, *A7* and *A8*.

4.1.2. Simplified Equations for Natural Frequencies and Mode Shapes

Segmented beam model was used to determine cutting tool dynamics. This beam model can be used in many areas. However, the calculations of the natural frequencies and mode shapes are very difficult because of the complex coefficient matrix (4.13). Simplified equations are developed to calculate the solution of the characteristic equation easily. The solution of the determinant of the complex coefficient matrix can be repeated for various segmented beam geometries. The natural frequency equations of segmented beam (4.16) can be rewritten in the following form:

$$\begin{aligned} &\omega = (\alpha L1)^2 \sqrt{\frac{EI1}{\rho A1 L1^4}} \quad \text{or} \quad \omega = (\beta L2)^2 \sqrt{\frac{EI2}{\rho A2 L2^4}} \\ &\omega = K \sqrt{\frac{EI1}{\rho A1 L1^4}} = \left(K \frac{d1}{d2} \frac{L2^2}{L1^2} \right) \sqrt{\frac{EI2}{\rho A2 L2^4}} \end{aligned} \tag{4.17}$$

In derivation of the equations to determine *K*, the length ratio (*L1/L2*) and the diameter ratio (*D1/D2*) are used. Therfore, the *K* value can be calculated for any given geometric properties. The graph for the variation in the *K* value for first mode according to *L1/L2* and *D1/D2* ratio is shown in Figure 4.2.

In Figure 4.2, the relation between *1/K* and *D1/D2* is linear. The slope and the constant of the line change according to *L1/L2* ratio. In order to calculate the natural frequency of the first mode, the equation between *K* and geometric properties is derived.

$$\frac{1}{K} = a\left(\frac{D1}{D2}\right) + b \rightarrow K = \frac{1}{a\left(\frac{D1}{D2}\right) + b} \tag{4.18}$$

where

$$a = \frac{-0.817(\ln l) + 0.0167}{l}$$

$$b = 0.1821l^2 + 0.1063l - 0.0275$$

$$l = \frac{L1}{L2}$$

The graph given in Figure 4.2, or equation 4.18, can be used to determine K based on L1/L2 and D1/D2 for any segmented beam with two sections.

Then, the fundamental natural frequency can be determined from equation 4.17 eliminating the need for eigenvalue solution for matrix (4.13). Therefore, the fundamental frequency of a segmented beam can be determined analytically, which is an original contribution. The application of this formulation to end mill dynamics is presented in chapter 6.

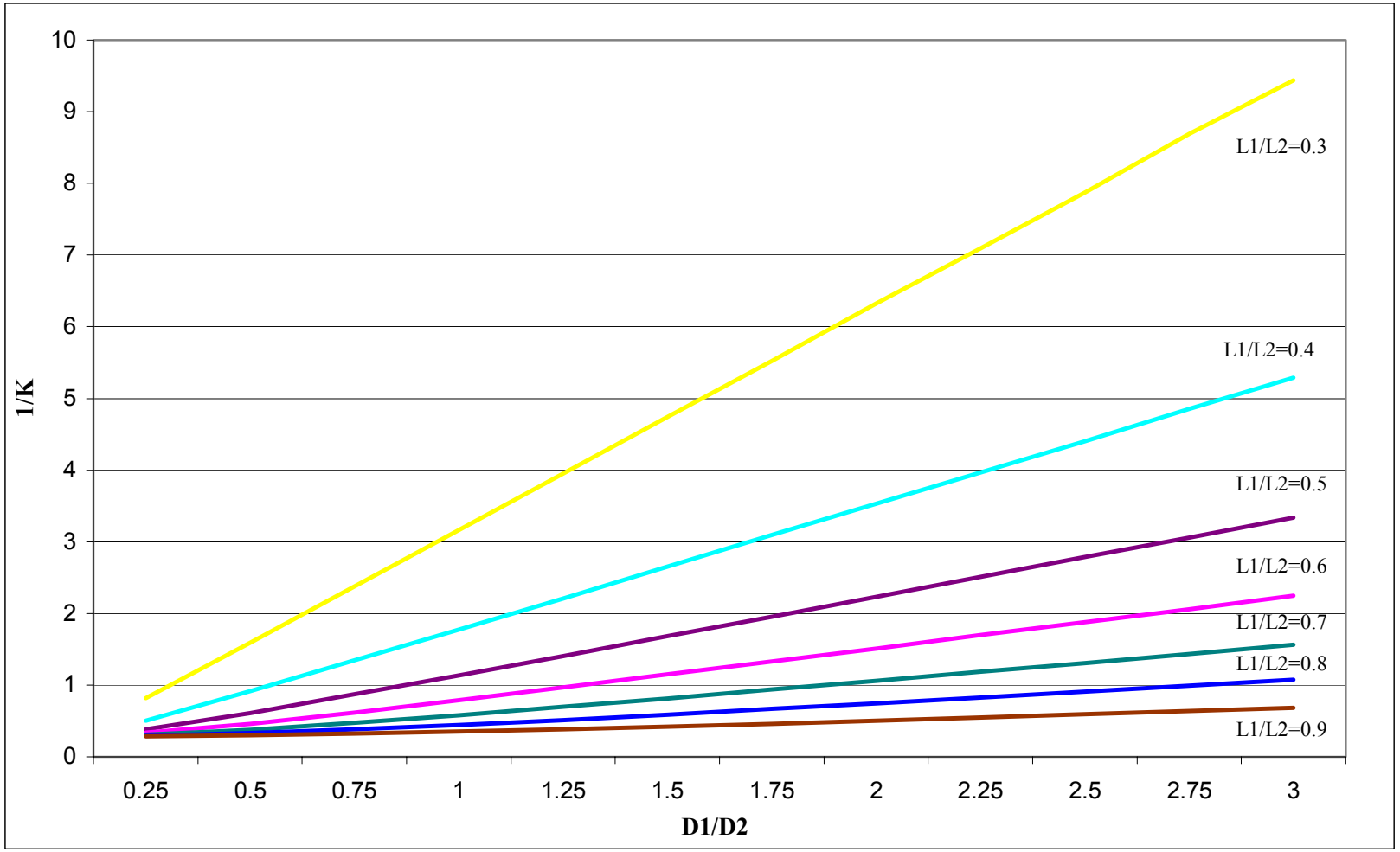

Figure 4.2: Relation between 1/K and D1/D2 ratio according to L1/L2 ratio

4.2. Modeling and FEA Analysis

In I-DEAS, models are built to define geometry, material properties, element types and constraints for end mills. Natural frequencies and mode shapes are obtained using FEA. (Shih, 2000)

4.2.1. Tool

Many end mills with different material and geometric parameters are analyzed. As an example, natural frequencies and mode shapes of a HSS end mill with 4-Flute, 16 mm diameter and 92 mm length are shown in Figure 4.3.

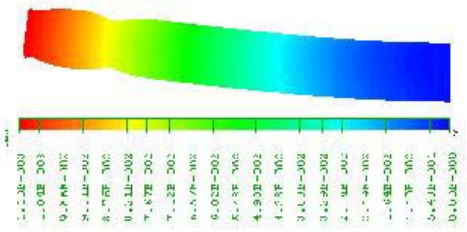

Mode1: 1476 Hz

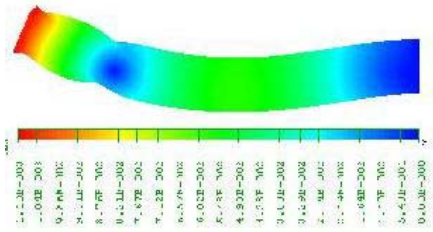

Mode2: 7134 Hz

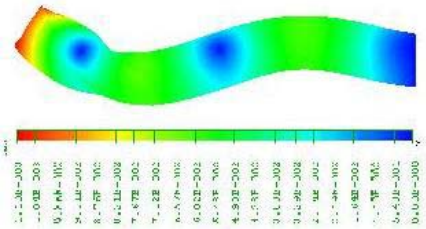

Mode3: 16764 Hz

Figure 4.3: Example of natural frequencies and mode shapes of a tool

The natural frequencies of HSS tools according to geometric properties of the end mill and frequency description are given in Table 4.1. The lateral and vertical bending frequencies are different for 2-flute cutter. The cross section of the 2-flute cutter is not symmetric with respect to x and y-axes, so the moment of inertia I_{xx} and I_{yy} are different.

Frequency (Hz)		D_1=6 mm, L_1=13 mm, L_2=57 mm, D_2=6 mm			D_1=10 mm, L_1=22 mm, L_2=72 mm, D_2=10 mm			D_1=16 mm, L_1=32 mm, L_2=92 mm, D_2=16 mm			D_1=20 mm, L_1=38 mm, L_2=104 mm, D_2=20 mm		
DESCRIPTION	**TYPE**	4_Flute	3_Flute	2_Flute	4_Flute	3_Flute	2_Flute	4_Flute	3_Flute	2_Flute	4_Flute	3_Flute	2_Flute
First Bending	X	1409	1500	1435	1504	1620	1534	1476	1600	1505	1443	1565	1468
First Bending	Y	1409	1500	1437	1504	1620	1539	1476	1600	1516	1443	1565	1483
Second Bending	X	7890	8072	7846	7755	7662	7475	7134	6897	6729	6800	6477	6328
Second Bending	Y	7890	8072	8005	7755	7662	7918	7134	6897	7331	6800	6477	6969
Third Bending	X	19604	18939	18623	18543	19218	18643	16764	15918	15671	15798	15009	14782
Third Bending	Y	19604	18939	19992	18543	19218	19018	16764	15918	17218	15798	15009	16214

Table 4.1: Natural frequencies (I-DEAS) of HSS end mills with different geometry

As the tool length/diameter ratio increases, the natural frequency of the tool decreases (Figure 4.4). 2-flute cutters have the greatest natural frequency and 4-flute cutters have the least because of the cross section. The natural frequencies of the cylinder that has the same diameter and length with other tools are also calculated. This graph shows that considering the tool as a cylinder is a bad approximation.

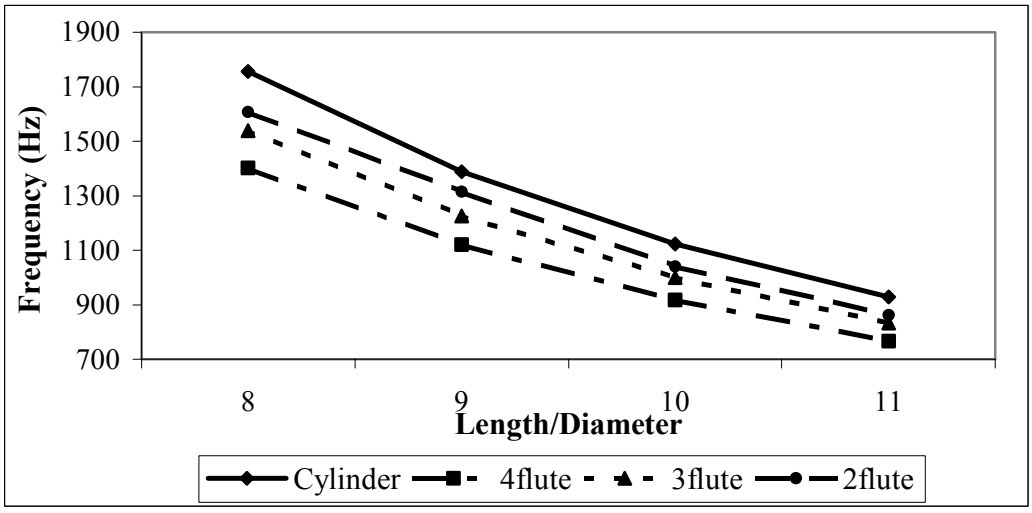

Figure 4.4: Relationship between natural frequencies (Mode1) of HSS tool and tool length/diameter ratio

Frequency (Hz)		D_1=6 mm, L_1=13 mm, L_2=57 mm, D_2=6 mm			D_1=10 mm, L_1=22 mm, L_2=72 mm, D_2=10 mm			D_1=16 mm, L_1=32 mm, L_2=92 mm, D_2=16 mm			D_1=20 mm, L_1=38 mm, L_2=104 mm, D_2=20 mm		
DESCRIPTION	**TYPE**	4_Flute	3_Flute	2_Flute	4_Flute	3_Flute	2_Flute	4_Flute	3_Flute	2_Flute	4_Flute	3_Flute	2_Flute
First Bending	X	2033	2164	2069	2169	2340	2210	2129	2309	2154	2082	2258	2118
First Bending	Y	2033	2164	2072	2169	2340	2221	2129	2309	2187	2082	2258	2139
Second Bending	X	11381	11646	11033	11187	11081	10922	10291	9950	10026	9765	9343	9033
Second Bending	Y	11381	11646	11549	11187	11081	11423	10291	9950	10575	9765	9343	10054
Third Bending	X	28282	27322	27624	26750	27727	26238	24189	22968	23657	22791	21655	22185
Third Bending	Y	28282	27322	28841	26750	27727	27436	24189	22968	24838	22971	21655	23391

Table 4.2: Natural frequencies (I-DEAS) of carbide end mills with different geometry

The lateral and vertical bending frequencies of carbide tools according to geometric properties and frequency description are given in Table 4.2. The carbide tools have higher natural frequency than HSS tools because of their high modulus of elasticity (Figure 4.5).

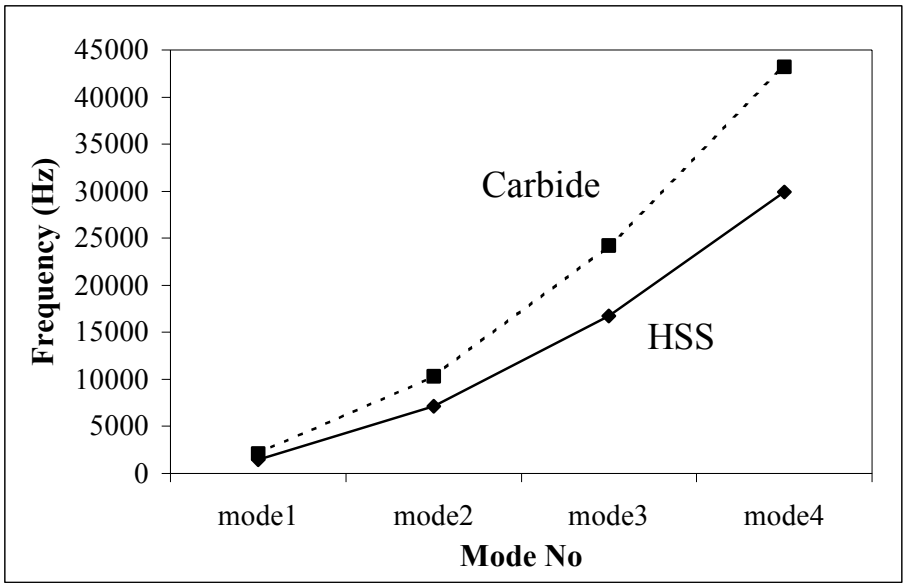

Figure 4.5: Comparison between carbide and HSS natural frequencies

4.2.2. Tool Holder

The dynamic characteristics of HSK (HSK-40, HSK-50 and HSK-63) and CAT (CAT-40 and CAT-50) tool holders were analyzed in I-DEAS. The first and second natural frequencies of tool holders are summarized in Table 4.3.

	First Bending (kHz)		Second Bending (kHz)	
Tool Holder Type	Lateral	Vertical	Lateral	Vertical
HSK-A40	14.74	14.76	20.50	20.70
HSK-A50	13.66	13.67	31.61	31.64
HSK-A63	13.85	13.87	28.48	28.56
CAT-40	8.05	8.06	22.73	22.73
CAT-50	7.19	7.20	21.70	21.71

Table 4.3: Results of the FEA for the tool holders in I-DEAS

4.3. Comparison of the Results from Finite Element Analysis and Analytic Solution

Analytic equations, which are used to predict dynamic behavior of the cutting tools, are compared with I-DEAS finite element analysis. Table 4.4 shows the error between the I-DEAS FE and analytic solution for 4-flute HSS end mill, which has 6 mm flute diameter, 13 mm flute length, 57 overall length and 6 mm in shank diameter. From Table 4.4, the error between FEM frequency and analytic calculated frequency increases from % 5 for mode1 to % 18 for mode 3.

4_FLUTE	**Frequency_Analytic (Hz)**	**Frequency_I-DEAS (Hz)**	**ERROR (%)**
First Bending	1409	1476	**4.74**
Second Bending	7890	8530	**8.12**
Third Bending	19601	23170	**18.21**

Table 4.4: Comparison of the natural frequencies of FE and analytic analysis

Table 4.5 shows the displacement errors between the I-DEAS FE and analytic analysis for the fist three modes. The mode shapes representations, which are drawn using analytic equations, are given in Table 4.5 for three modes of the 4-flute cutting tool. Critical displacements values and their positions along the tool length are compared. The error in maximum displacement is in the range of % 3.5 - %12.5. As tool diameter and tool length increases, the error in the natural frequencies between FEM and analytic model.

4_Flute (I-DEAS)		**ANALYTIC**		
x/L	Displacement (mm)	**x/L**	Displacement (mm)	**ERROR (%)**
0	0.0000	**0**	0.0000	**-**
1/4	0.1138	**1/4**	0.1147	**0.79**
2/4	0.4100	**2/4**	0.3943	**3.83**
3/4	0.7860	**3/4**	0.7541	**4.06**
1	1.1770	**1**	1.1365	**3.44**

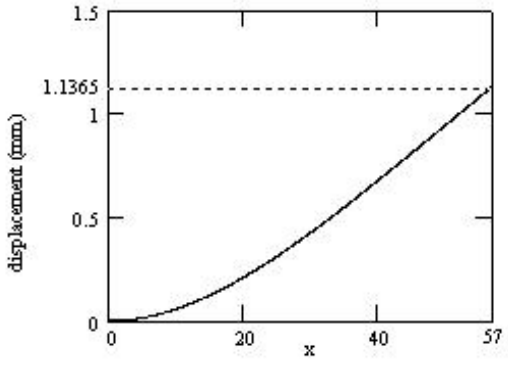

a) Mode 1

4_Flute (I-DEAS)		**ANALYTIC**		
x/L	Displacement (mm)	**x/L**	Displacement (mm)	**ERROR (%)**
0	0.0000	**0**	0.0000	**-**
A/L=0,456	0.7403	**A/L=0,448**	0.7738	**4.52**
B/L=0,761	0.0000	**B/L=0,742**	0.0000	**-**
C/L=1	1.3450	**C/L=1**	1.4301	**6.33**

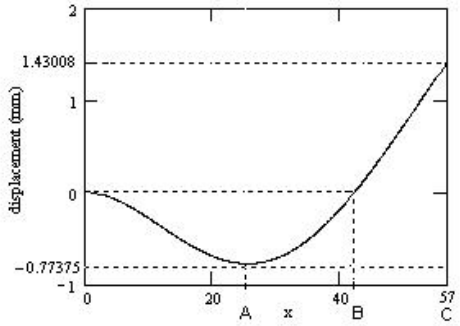

b) Mode 2

4_Flute (I-DEAS)		ANALYTIC		
x/L	Displacement (mm)	**x/L**	Displacement (mm)	**ERROR (%)**
0	0.0000	**0**	0.0000	**-**
A/L=0,283	0.6490	**A/L=0,282**	0.6509	**0.30**
B/L=0,5	0.0000	**B/L=0,488**	0.0000	**-**
C/L=0,7	0.5870	**C/L=0,672**	0.5655	**3.66**
D/L=0,867	0.0000	**D/L=0,842**	0.0000	**-**
E/L=1	1.2360	**E/L=1**	1.0827	**12.40**

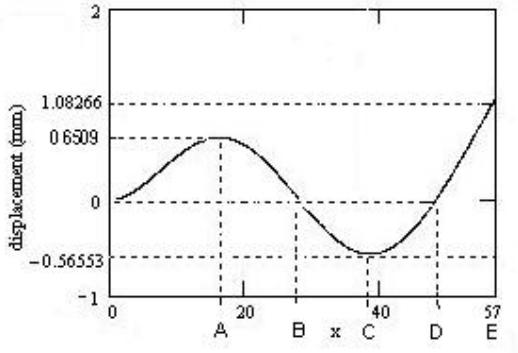

c) Mode 3

Table 4.5: Comparison of the mode shapes of FE and analytic analysis

4.4. Experimental Method

4.4.1. Testing and Analysis

Complete dynamic description of the machine requires the determination of modal frequencies, mode shapes and system parameters (equivalent mass, stiffness and damping ratio). Experimental modal analysis deals with a method of measuring the response of a machine, structure or system to vibration and using that information to identify some of its dynamic properties. The response of a system can be measured in terms of its displacement, velocity, or acceleration.

FRF (Frequency Response Function) plays an important role in the experimental modal analysis. The frequency response function is first determined experimentally and then analyzed to find the natural frequencies, mode shapes and system parameters. The system parameters (equivalent mass, stiffness and damping ratio) can be used to predict the response of the system to various excitations.

General arrangement the can be for the frequency response measurement of system is shown in Figure 4.6. A hammer is used to apply an impact load at different points of the system while an accelerometer is fixed at one location to measure the response. Testing the functional transfer and transactional characteristics of a mechanical structure involves mounting the accelerometer at one location of interest and striking the object with hammer at that point or some other point.

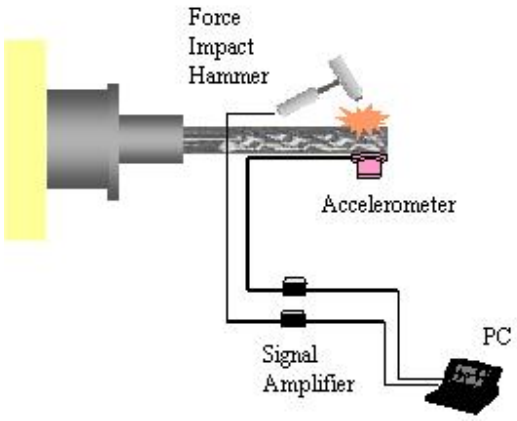

Figure 4.6: FRF measurement system

The hammer consists of an integral, quartz force sensor mounted on the striking end of the hammer head. The sensing element functions to transfer impact force into electrical signal for display and analysis. Signals generated by accelerometer and hammer are powdered by conditioning amplifiers. These sensors are easy to operate and interface with signal analysis, data acquisition and recording instruments.

Time response of the accelerometer is measured, but the same data must be converted into frequency domain. Fast Fourier Transform (FFT) is used to convert the time data. Computers can be used to collect to the data, estimate the modal parameters and display the results. Small desktop computers are available along with user-friendly programs to guide the user through all the steps of modal testing. In this research, the data is collected by CutPro© MalTF software where the modal analysis is also performed in CutPro© Modal (Alitntas, 2000).

The FRFs indicates the dynamic characteristics of a system. A plot (Figure 4.7) of a FRF provides the approximate values of natural frequencies and damping ratios. In some cases, a set of FRFs can be used to find an approximate mode shape.

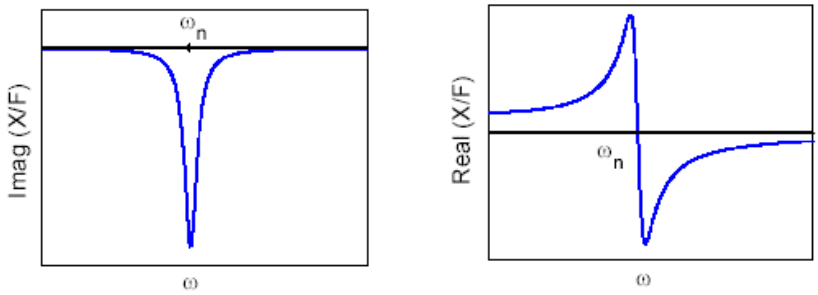

Figure 4.7: The graph of real and imaginary part of FRF

4.4.2. Example

The analytic solution is very useful to identify the dynamic properties of the tools. In this section, the analytical FRF prediction method is compared with the results obtained from experiments.

4-flute carbide end-mill with long overhang is selected to demonstrate the accuracy of analytical results. The mill and shank diameter is 8 mm, the flute length is 41 mm and the gauge length is 80 mm. FRF measurement was performed to determine the transfer function of the end mill, which is shown in Figure 4.7. Table 4.6 shows the identified frequency, stiffness, damping and mass values for the end mill. For comparison with analytical model predictions, the results obtained using the cylinder approximation for the end mill are also shown in Table 4.6 and Figure 4.7. The cylinder with the same diameter and length is used in calculations. The graphs between the magnitude of the transfer function and frequency for all methods are shown in Figure 4.7.

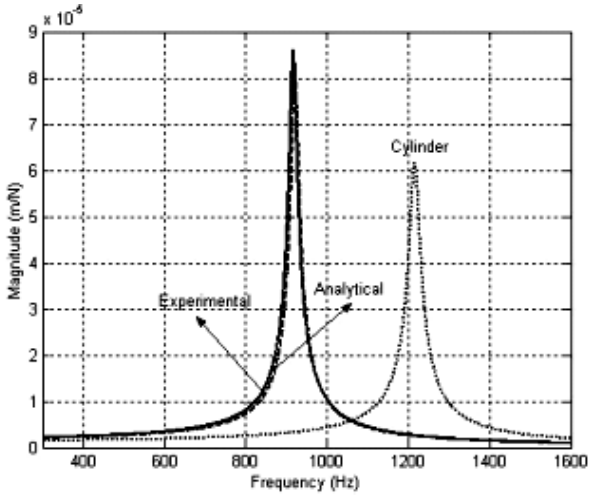

Figure 4.7: Magnitude of the transfer function for the experimental, I-DEAS, analytical and cylinder methods

Transfer Function	Frequency (Hz)	Stiffness (N/m)	Damping (ζ)	Mass (kg)
Experiment	935	5.11E+5	0.012	0.0150
Analytic Solution	922	5.50E+5	0.012	0.0164
Cylinder	1216	7.12E+5	0.012	0.0122

Table 4.6: The comparison of the dynamic properties obtained from experimental, analytical and cylinder methods

Due to the long flute length of the tool, the cylinder approximation is very poor in this case. The approximation results could be improved by using an effective diameter for the cylinder. As the end mills do not have circular cross sections along the flute length, the analytical solution is the most powerful approximation to find the dynamic properties. The model presented in this chapter can be used to determine the dynamics of end mills for a given geometry, material and clamping conditions.

4.5. Summary

In this chapter, a method of modeling for transverse vibrations of geometrically segmented beam is proposed. End mill is assumed to be as segmented beam with one end fixed and other end free. In order to obtain natural frequency and mode shape of the system, complex matrix calculations are needed. Simplified equations are derived to eliminate time consuming calculations. In these equations, desired geometric properties can be selected for prediction..

Finite Element Analysis (FEA) results of various tool geometries, different materials and tool holder types are given. These results are compared with the results obtained from analytic equations.

Frequency Response Function (FRF) measurements need to be performed to identify the dynamics of the system experimentally. Transfer function measurement system and modal analysis are described.

CHAPTER 5

CLAMPING PARAMETERS FOR END MILLS

Complete dynamic response of an end mill depends on the machine, tool holder and end mill component dynamics as well as the interface or contact parameters among them. In this study, the dynamic characteristics at the tip of the holder, which involves the dynamics of both spindle and holder, are assumed to be known from experimental data. Considering small number of spindle/holder combination compared to holder/tool combination, this is an acceptable approach. The tool dynamics are calculated analytically. The next important parameter for the prediction of the total dynamics of the system is the interface or contact parameters (stiffness and damping) between the tool and the holder.

The application of receptance coupling substructure analysis to the analytic prediction of tool point dynamic response is described. Tool point dynamic response is predicted by using frequency response measurements of individual components coupled though appropriate connections.

In the first section, the description of receptance coupling substructure analysis (RCSA) and a method to identify the connection parameters (stiffness and damping) between tool and tool holder/ spindle are given. The effects of changes in tool parameters and clamping conditions are explained with experimental results in the second section.

5.1. Method for Identification of the Connection Parameters Tool and Tool Holder/Spindle

Complete machine structure is divided into two parts, tool and tool holder/spindle. The description of the assembly model and the connection parameters are shown in Figure 5.1. (Schmitz, 2000)

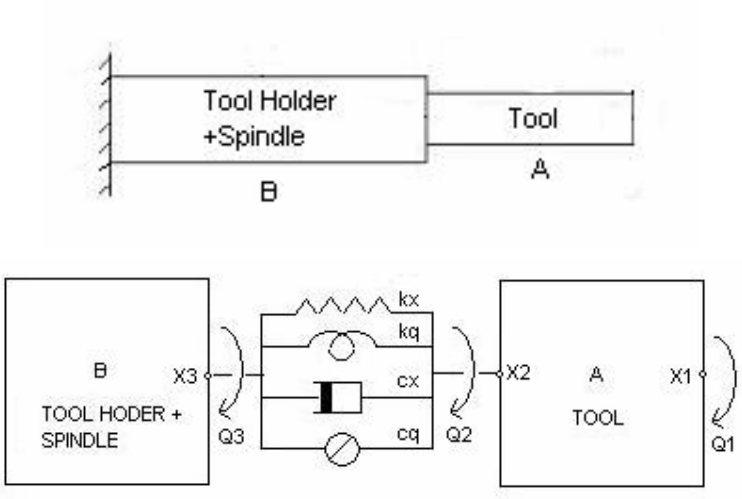

Figure 5.1: Tool and tool holder/spindle assembly

The four connection parameters (linear and torsional springs and dampers) must be determined to predict tool point frequency response function (FRF). According to these parameters, tool and tool holder/spindle FRFs are coupled using receptance coupling substructure analysis (RCSA). RCSA is a very efficient analysis to predict tool point dynamic response without the measurement of each tool, tool holder and spindle combination. In receptance coupling substructure analysis, experimental or analytical direct and cross FRFs for individual components are used to predict the final assembly's dynamic response at any spatial coordinate selected for component measurements. In this method, experimental or analytical FRFs are required only at the coordinate of interest and any connection coordinates.

In RCSA, each component of the assembly must be tested separately to determine the component FRFs. Nevertheless, this is only possible if the impact tests on the individual parts provide enough information to predict accurately the dynamic properties of the assembled structure. In case of low natural frequency modes, the dynamics at the tool and tool holder/spindle interface might not be adequately represented in the modal data. Furthermore, in many cases the measurement of component dynamics is not practical which is the case for free-free end mill. Free-free state is difficult to realize in practice. The direct and cross free-free state FRFs for coordinates of component A are calculated analytically. An analytical formulation, rather than experimental measurement, was selected due to the difficulties associated with obtaining these tool FRFs using impact test. The direct FRFs at coordinate x_3 of the component B are obtained experimentally using impact testing. The holder/spindle component is difficult to model analytically.

The holder and spindle dynamic properties can also be determined using FEA (Kıvanc and Budak, 2003, Jorgensen and Shin, 1998). However, the number of spindle/holder combinations for milling tools is much more limited on a machining center, and thus they can be measured and used for different end mill combinations. In order to evaluate the FRF of the tool/holder/spindle system, the end mill can be modeled using a standard finite element (FE) model of a cylindrical beam and the FRF of the holder/spindle system is identified using impact testing (Park and Altintas, 2003)

The receptance term, G, for the assembled system in Figure 5.2 will be derived by using the receptance coupling method. Figure 5.2 displays the assembled and component systems with F_1 (force) and M_1 (moment) applied to the assembled system. The direct deflection receptance $G_{11}(\omega) = \frac{X_1}{F_1}$ for the combined spindle/holder/tool structure C.

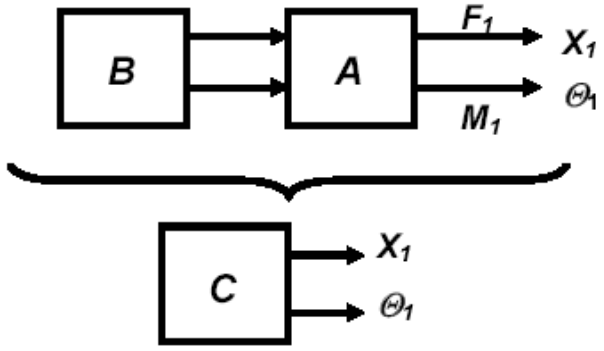

Figure 5.2: Assembled spindle/holder/tool structure

Considering the (unassembled) substructures in Figure 5.3 the displacements and rotations can be written. The notation H refers to receptance term (displacement over force). The direct FRFs at coordinates x_1 and x_2 (H_{11} and H_{22}, respectively) and a cross FRF H_{12} (H_{21} is equivalent by reciprocity) can be derived by analytically. For this model, response functions that relate displacement under applied moment (L_{mn}), rotation under applied force (N_{mn}) and the rotation under applied moment (P_{mn}) are also included. The terms H'_{mn}, L'_{mn}, N'_{mn} *and* P'_{mn} represent mobility FRFs, or the ratio of linear or rotational velocity to force or moment. The linear and rotational stiffness and damping terms are labeled k_x, k_θ, c_x and c_θ, respectively.

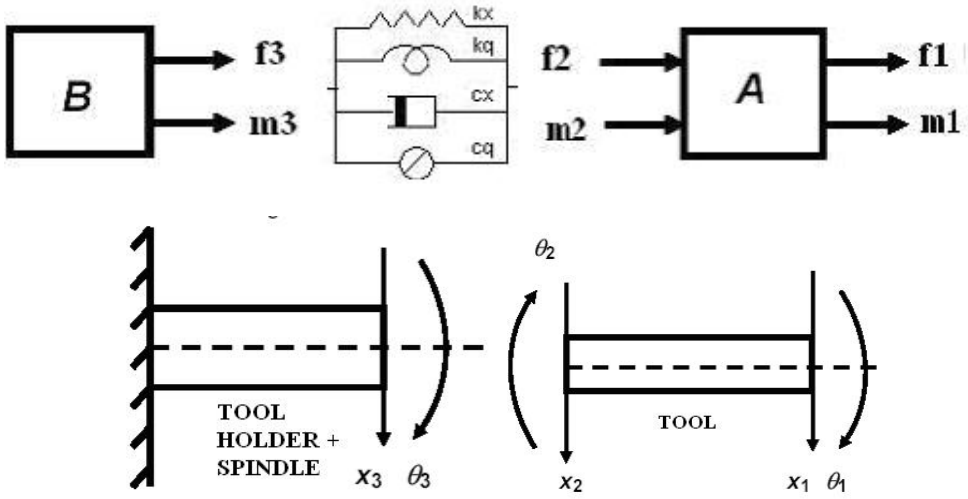

Figure 5.3:Componenets of the spindle/holder/tool structure

The displacement and rotation conditions at coordinates x_1, x_2 and x_3 for the components and at X_1 for the assembly are given in equations 5.1 and 5.2.

$$\begin{aligned}
x_1 &= H_{11}f_1 + L_{11}m_1 + H_{12}f_2 + L_{12}m_2 \\
\theta_1 &= N_{11}f_1 + P_{11}m_1 + N_{12}f_2 + P_{12}m_2 \\
x_2 &= H_{21}f_1 + L_{21}m_1 + H_{22}f_2 + L_{22}m_2 \\
\theta_2 &= N_{21}f_1 + P_{21}m_1 + N_{22}f_2 + P_{22}m_2 \\
x_3 &= H_{33}f_3 + L_{33}m_3 \\
\theta_3 &= N_{33}f_3 + P_{33}m_3
\end{aligned} \tag{5.1}$$

$$\begin{aligned}
X_1 &= H_{11}F_1 + L_{11}M_1 + H_{12}f_2 + L_{12}m_2 \\
\Theta_1 &= N_{11}F_1 + P_{11}M_1 + N_{12}f_2 + P_{12}m_2
\end{aligned} \tag{5.2}$$

The force and moment equilibrium condition for components is given in equation 5.3. The compatibility conditions are shown in equation 5.4.

$$\begin{aligned}
&f_2 + f_3 = 0 \rightarrow f_3 = -f_2 \\
&m_2 + m_3 = 0 \rightarrow m_3 = -m_2 \\
&X_1 = x_1, \quad \Theta_1 = \theta_1
\end{aligned} \tag{5.3}$$

$$\begin{aligned}
&k_x(x_3 - x_2) + c_x(x_3' - x_2') = f_2 \\
&k_q(\theta_3 - \theta_2) + c_q(\theta_3' - \theta_2') = m_2
\end{aligned} \tag{5.4}$$

Substitution of equations of the displacement (x_2 and x_3), the rotation (θ_2 and θ_3) at coordinates x_2 and x_3, their derivatives (x_2', x_3', θ_2', θ_3') and equation 5.3 into equation 5.4 yields equation 5.5.

$$\begin{aligned}
&(k_xH_{33} + k_xH_{22} + c_xH_{33}' + c_xH_{22}' + 1)f_2 + \\
&(k_xL_{33} + k_xL_{22} + c_xL_{33}' + c_xL_{22}')m_2 = -k_xH_{21}F_1 - k_xL_{21}M_1 - c_xH_{21}'F_1 - c_xL_{21}'M_1 \\
&(k_qN_{33} + k_qN_{22} + c_qN_{33}' + c_qN_{22}')f_2 + \\
&(k_qP_{33} + k_qP_{22} + c_qP_{33}' + c_qP_{22}' + 1)m_2 = -k_qN_{21}F_1 - k_qP_{21}M_1 - c_qN_{21}'F_1 - c_qP_{21}'M_1
\end{aligned} \tag{5.5}$$

There are two unknowns and two equations. The expressions for the force and moment acting on individual component (f_2, m_2, f_3=- f_2 and m_3=- m_2) can be evaluated from equation 5.5.

$$\begin{aligned} &Af_2 + Bm_2 = C_1 \\ &E_4 f_2 + E_3 m_2 = C_2 \\ &f_2 = \frac{E_3 C_1 - C_2 B}{E_4 B - A E_3}, \quad m_2 = \frac{-AC_2 + C_1 E_4}{E_4 B - A E_3} \end{aligned} \tag{5.6}$$

where

$$\begin{aligned} A &= k_x H_{33} + k_x H_{22} + c_x H_{33}' + c_x H_{22}' + 1 \\ B &= k_x L_{33} + k_x L_{22} + c_x L_{33}' + c_x L_{22}' \\ E_3 &= k_q P_{33} + k_q P_{22} + c_q P_{33}' + c_q P_{22}' + 1 \\ E_4 &= k_q N_{33} + k_q N_{22} + c_q N_{33}' + c_q N_{22}' \\ C1 &= -k_x H_{21} F_1 - k_x L_{21} M_1 - c_x H_{21}' F_1 - c_x L_{21}' M_1 \\ C2 &= -k_q N_{21} F_1 - k_q P_{21} M_1 - c_q N_{21}' F_1 - c_q P_{21}' M_1 \end{aligned} \tag{5.7}$$

From equation 5.2, the direct deflection receptance $G_{11}(\omega) = \frac{X_1}{F_1}$ for assembled spindle/holder/tool structure C can be determined.

$$\begin{aligned} &X_1 = H_{11} F_1 + L_{11} M_1 + H_{12} f_2 + L_{12} m_2 \\ &X_1 = \left(H_{11} + H_{12} \frac{f_2}{F_1} + L_{12} \frac{m_2}{F_1} \right) F_1 + \left(L_{11} H_{12} \frac{f_2}{M_1} + L_{12} \frac{m_2}{M_1} \right) M_1 \end{aligned} \tag{5.8}$$

The terms, $\frac{f_2}{F_1}$ and $\frac{m_2}{F_1}$ must be calculated in order to evaluate the term, X_1 / F_1. By using equation 5.6, equation 5.9 and 5.10 can be derived.

$$f_2 = \frac{E_3 C_1 - C_2 B}{E_4 B - A E_3}$$

$$f_2 = \frac{E_3(-k_x H_{21} F_1 - k_x L_{21} M_1 - c_x H_{21}' F_1 - c_x L_{21}' M_1) - B(-k_q N_{21} F_1 - k_q P_{21} M_1 - c_q N_{21}' F_1 - c_q P_{21}' M_1)}{E_4 B - A E_3}$$

$$f_2 = \frac{[-E_3(k_x H_{21} + c_x H_{21}') + B(k_q N_{21} + c_q N_{21}')] F_1}{E_4 B - A E_3} + (\ ....) M_1$$

$$\frac{f_2}{F_1} = \frac{[(k_x H_{21} + c_x H_{21}') - E_3^{-1} B(k_q N_{21} + c_q N_{21}')]}{E_3^{-1} E_4 B - A}$$

$$\frac{f_2}{F_1} = (E_2 E_1^{-1})$$

where

$$E_1 = E_3^{-1} E_4 B - A$$

$$E_2 = (k_x H_{21} + c_x H_{21}') - E_3^{-1} B(k_q N_{21} + c_q N_{21}')$$

(5.9)

$$m_2 = \frac{-A C_2 + C_1 E_4}{E_4 B - A E_3}$$

$$m_2 = \frac{-A(-k_q N_{21} F_1 - k_q P_{21} M_1 - c_q N_{21}' F_1 - c_q P_{21}' M_1) + E_4(-k_x H_{21} F_1 - k_x L_{21} M_1 - c_x H_{21}' F_1 - c_x L_{21}' M_1)}{E_4 B - A E_3}$$

$$m_2 = \frac{[A(k_q N_{21} + c_q N_{21}') - E_4(k_x H_{21} + c_x H_{21}')] F_1}{E_4 B - A E_3} + (....) M_1$$

$$\frac{m_2}{F_2} = \frac{E_3^{-1}[A(k_q N_{21} + c_q N_{21}') - E_4(k_x H_{21} + c_x H_{21}')]}{E_3^{-1} E_4 B - A}$$

$$\frac{m_2}{F_2} = E_3^{-1}\left[E_4 E_2 E^{-1} - (k_q N_{21} + c_q N_{21}') \right]$$

(5.10)

Substitution of equation 5.9 and 5.10 into 5.8 give the expression for the G_{11} receptance term. Finally, after RCSA for the complete structure, the analytical displacement/force relationship at the tool tip (G_{11}), which is required for stability and chatter avoidance, is given as (Schmitz, et. al, 2001):

$$G_{11} = \frac{X_1}{F_1} = H_{11} - H_{12} E_1^{-1} E_2 - L_{12} E_3^{-1}((k_\theta N_{21} + c_\theta N_{21}') - E_4 E_1^{-1} E_2) \quad (5.11)$$

where

$$
\begin{aligned}
E_1 &= (k_x H_{33} + k_x H_{22} + c_x H'_{33} + c_x H'_{22} + 1) - E_3^{-1} E_4 (k_x L_{33} + k_x L_{22} + c_x L'_{33} + c_x L'_{22}) \\
E_2 &= (k_x H_{21} + c_x H'_{21}) - E_3^{-1} (k_\theta N_{21} + c_\theta N'_{21})(k_x L_{33} + k_x L_{22} + c_x L'_{33} + c_x L'_{22}) \\
E_3 &= k_\theta P_{33} + k_\theta P_{22} + c_\theta P'_{33} + c_\theta P'_{22} + 1 \\
E_4 &= k_\theta N_{33} + k_\theta N_{22} + c_\theta N'_{33} + c_\theta N'_{22} \\
H'_{mn} &= iwH_{mn},\ L'_{mn} = iwL_{mn} \\
N'_{mn} &= iwN_{mn},\ P'_{mn} = iwP_{mn}
\end{aligned}
\tag{5.12}
$$

The receptance term (H) contains three components. The first represent the contributions by transnational and rotational rigid body modes, respectively. The third gives response due to the free-free modes $\phi_I(x)$, expressed as shown in equation 5.17, which are evaluated at coordinate x_1 (a distance L from the model origin). For the tool holder/spindle component the direct deflection receptance term (H_{33}) is measured at the intersection location by impact test.

$$
\begin{aligned}
H_{11} &= \frac{-1}{m\omega^2} + \frac{-3}{m\omega^2} + \sum_{i=1}^{\infty} \left[\frac{\phi_i(L)^2}{-m\omega^2 + ic\omega + \frac{EI\lambda_i^4}{L^3}} \right] \\
H_{22} &= \frac{-1}{m\omega^2} + \frac{-3}{m\omega^2} + \sum_{i=1}^{\infty} \left[\frac{\phi_i(0)\phi_i(L)}{-m\omega^2 + ic\omega + \frac{EI\lambda_i^4}{L^3}} \right] \\
H_{21} &= -H_{12} \\
H_{22} &= \frac{-1}{m\omega^2} + \frac{-3}{m\omega^2} + \sum_{i=1}^{\infty} \left[\frac{\phi_i(0)^2}{-m\omega^2 + ic\omega + \frac{EI\lambda_i^4}{L^3}} \right] \\
H_{33} &\rightarrow \text{Experimentally determined}
\end{aligned}
\tag{5.13}
$$

Response functions that relate displacement to applied moment are derived. For component B (tool holder/spindle combination), the direct FRF (L_{33}) pertaining moment at the connection point is required. It is assumed zero because of the absence of reliable measurement techniques.

$$L_{12} = \frac{-6}{mL\omega^2} + \sum_{i=1}^{\infty} \left[\frac{\phi_i'(0)\phi_i(L)}{-m\omega^2 + ic\omega + \frac{EI\lambda_i^4}{L^3}} \right]$$

$$L_{22} = \frac{6}{mL\omega^2} + \sum_{i=1}^{\infty} \left[\frac{\phi_i'(0)\phi_i(0)}{-m\omega^2 + ic\omega + \frac{EI\lambda_i^4}{L^3}} \right] \tag{5.14}$$

$L_{33} \rightarrow$ assummed zero

Response functions that relate rotation to applied force are shown in equation 5.15. The direct FRF at the connection coordinate (N_{33}) is assumed zero.

$$N_{21} = \frac{-6}{mL\omega^2} + \sum_{i=1}^{\infty} \left[\frac{\phi_i(L)\phi_i'(0)}{-m\omega^2 + ic\omega + \frac{EI\lambda_i^4}{L^3}} \right]$$

$$N_{22} = \frac{6}{mL\omega^2} + \sum_{i=1}^{\infty} \left[\frac{\phi_i(0)\phi_i'(0)}{-m\omega^2 + ic\omega + \frac{EI\lambda_i^4}{L^3}} \right] \tag{5.15}$$

$N_{33} \rightarrow$ assummed zero

Response functions that relate rotation to applied moment are also derived. For component B, the direct FRF *(P_{33})* pertaining moment is also assumed zero.

$$P_{22} = \frac{-12}{mL^2\omega^2} + \sum_{i=1}^{\infty} \left[\frac{\left(\phi_i'(0)\right)^2}{-m\omega^2 + ic\omega + \frac{EI\lambda_i^4}{L^3}} \right] \tag{5.16}$$

$P_{33} \rightarrow$ assummed zero

The response due to the free-free modes is shown in the following equation. λ_i is a dimensionless frequency parameter.

$$\phi_i(x) = \cosh\left(\frac{\lambda_i x}{L}\right) + \cos\left(\frac{\lambda_i x}{L}\right) - \sigma_i\left[\sinh\left(\frac{\lambda_i x}{L}\right) + \sin\left(\frac{\lambda_i x}{L}\right)\right]$$

$$\sigma_i = \frac{\cosh\lambda_i - \cos\lambda_i}{\sinh\lambda_i - \sin\lambda_i}$$

$$\lambda_i = \begin{Bmatrix} 4.7300 & \text{i=1} \\ 7.8532 & \text{i=2} \\ 10.9556 & \text{i=3} \\ 14.1371 & \text{i=4} \\ 17.2787 & \text{i=5} \\ (2i+1)\frac{\pi}{2} & \text{i} > 5 \end{Bmatrix} \tag{5.17}$$

For the calculations elastic modulus (E), viscous damping coefficient (c), mass (m) and second moment of inertia (I) are required. In the static analysis section, an analytic equation for the maximum displacement at the tool tip was derived which can be used to determine the stiffness of the tool (Chapter 3). The effective diameter of the tool and the second moment of inertia can be calculated using the analytical equations developed in Chapter 3 for segmented beam with different moments of inertias and the cantilever beam equation of the uniform cylinder. The mass of the tool can then be determined using the natural frequency and stiffness both from analytic equations. The damping ratios for different HSS and carbide tools have been determined experimentally. By using these dynamic properties, the approximate c values are estimated. Note that c values determined this way includes the damping of the tool only without the damping from the clamping as they are identified from end mill's component mode dynamics. These damping values can then be used in the analysis of different tools.

In experiments, the tool point FRFs (G_{11}) of the tool/tool holder/spindle assembly are measured for different tools. The connection parameters (k_x, k_θ, c_x, c_θ) are determined using *lsqnonlin* command of Matlab Optimization Toolbox [Schmitz and Burn, 2003, MatWorks, 2002]**.** *Isqnonlin* solves nonlinear least squares problems, including nonlinear data fitting. *X=lsqnonlin (fnctn,*X_o*)* starts at a point X_0 and finds a minimum to the sum of squares of the functions described in *fnctn*. Our syntax is [*X, resnorm, residual, exitflag, output]=lsqnonlin(fnctn ,*X_0*,lb, ub, options]*. The solution is always in the range *lb* <= *X* <=

ub. The optimization parameters (*max iteration number, max function evaluation number, tolerances for function and X values*) are specified in the structure options. The value of the residual for a solution *X*, the value *exitflag* (0,1) that describes the exit condition and the structure output that contains information about the optimization are returned. According to the calculated spring and damper parameters, the tool point FRF of the assembly is predicted analytically using Eq. (5.1). The experimentally measured result and the predicted results for G_{11} are compared in the next section.

5.2. Experimental Results

In this section, the FRFs using analytical models and the RCSA are compared with experimental results for verification. For the identification of the interface stiffness and damping between the tool and tool holder, different tool geometries, materials and clamping conditions are used. Contact parameters are identified and presented.

The tool holder/spindle direct FRF (H_{33}) is measured at the free end in *x/y* directions by using low mass accelerometer and impact hammer. The measured FRF for X direction of the HSK40 tool holder/spindle is shown in Figure 5.5. The same tool holder is used with different end mills, and therefore the same FRF (H_{33}) is used in RCSA in the following examples. Interaction between tool and tool holder/spindle modes affects the tool point FRF. Figure 5.4 shows the tool and tool holder/spindle assembly and variable tool geometry properties.

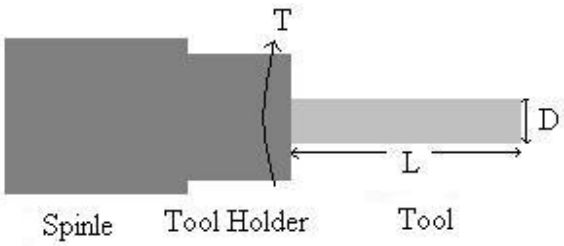

Figure 5.4: Tool- tool holder/spindle assembly and changing parameters

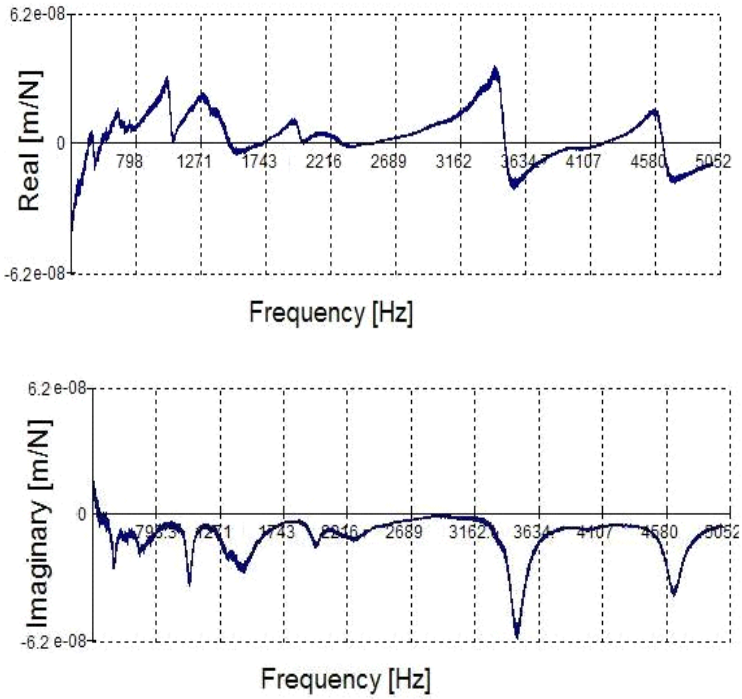

Figure 5.5: Measured FRF of tip of HSK40 tool holder/spindle combination (X direction)

5.2.1. The Effect of the Tool Length

A carbide end mill with 4 flutes, 8 mm diameter, and 100 mm length is used for test. Different lengths (length to diameter ratios of 8:1, 9:1, 10:1, 11:1) are selected for the measurement.25 Nm clamping torque is applied on HSK40 holder. The tool effective diameter and damping coefficient were determined as 7.49 mm and 20 Ns/m, respectively.

After the nonlinear least square evaluation, the stiffness and damping coefficients are determined as shown in Table 5.1**.** The change in predictive values of linear rotational stiffness and damping coefficients for the longest and shortest tools is shown in Figure 5.6. After the connection parameters are obtained, the analytic direct and cross FRFs for the tool and experimental holder/spindle direct FRF are inserted equation 5.1. Experimental impact tests were also performed for each of the four selected tools.

	L/D=8	L/D=9	L/D=10	L/D=11
	D=8, L=64, T=25, $L_{contact}$=36	**D=8, L=72, T=25, $L_{contact}$=28**	**D=8, L=80, T=25, $L_{contact}$=20**	**D=8, L=88, T=25, $L_{contact}$=12**
kx (N/m)	$9.036 * 10^6$	$6.885 * 10^6$	$3.614 * 10^6$	$1.304* 10^6$
kq (Nm/rad)	$1.02 * 10^7$	$5.3 * 10^6$	$3.8 * 10^6$	$1.277* 10^6$
cx (Ns/m)	445	368	228	141
cq (Nms/rad)	54.17	71.44	78.09	79.34

Table 5.1: Stiffness/ damping coefficients for 8 mm diameter for shortest and longest tools

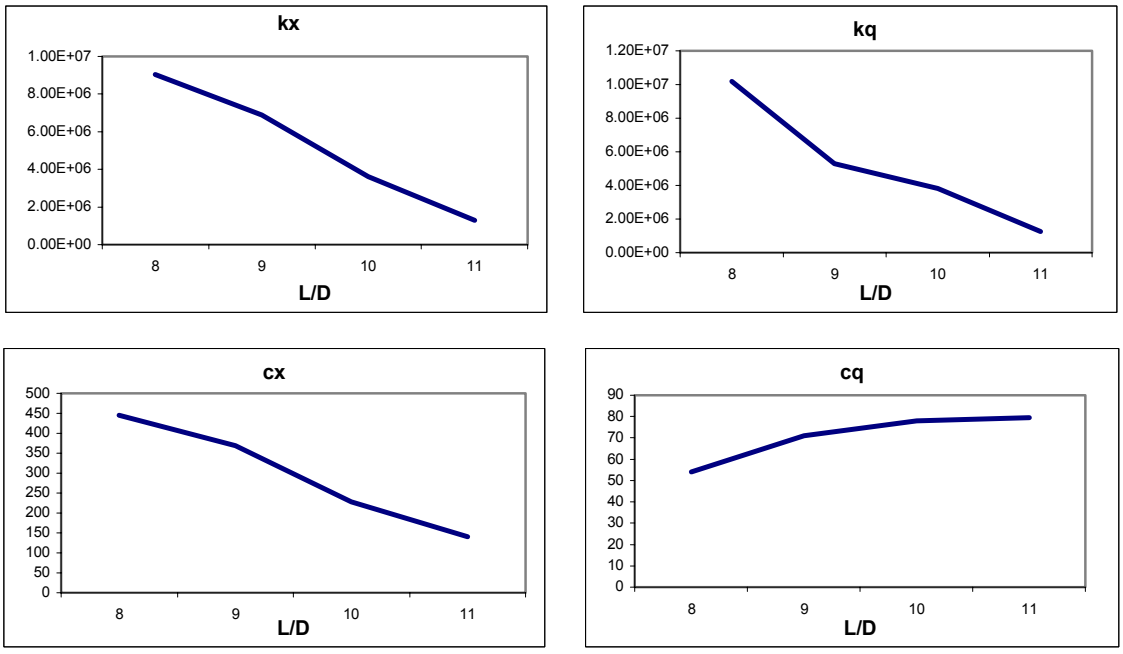

Figure 5.6: Variation of the connection parameters for shortest and longest tool

The measured and predicted FRFs using analytical component FRFs and RCSA are shown Figure 5.7 for different length to diameter ratios. The response is governed by only the first mode of the tool, and thus only the first beam mode is used in the analytical component modes. The agreement between the experimental results and the predictions is

satisfactory. For a tool, when the overhang is increased, contact length between tool and tool holder, natural frequency and stiffness decreases and tool flexibility increases.

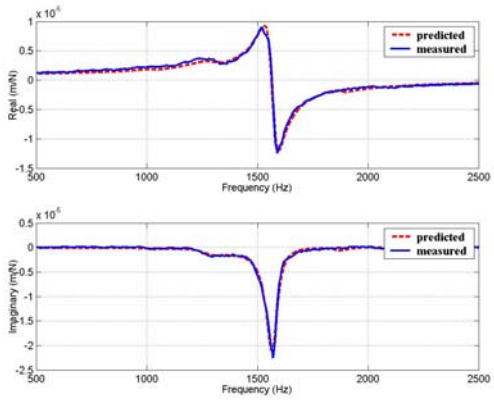

a) L/D = 8

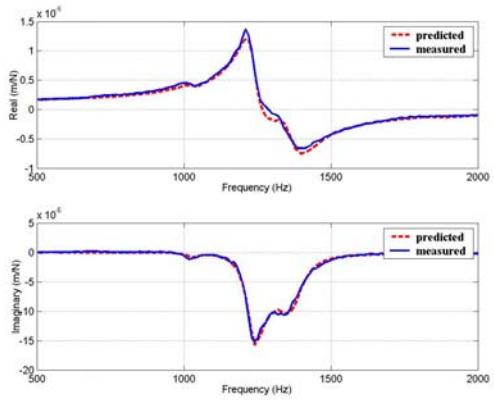

b) L/D = 9

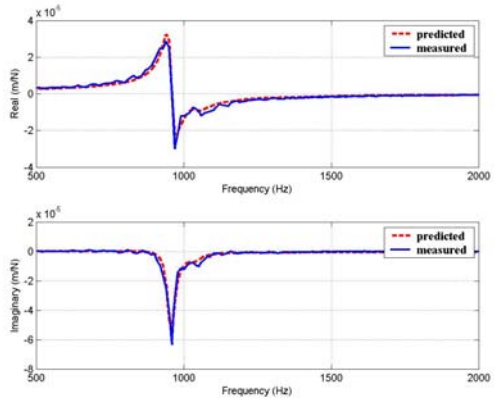

c) L/D = 10

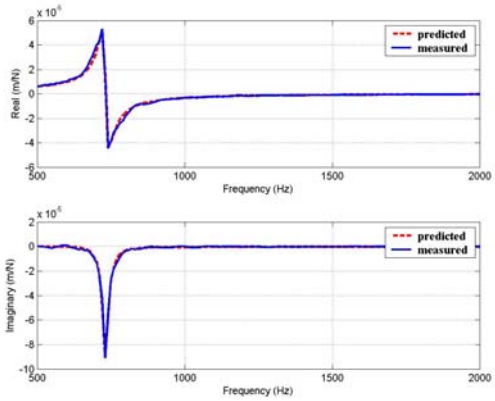

d) L/D = 11

Figure 5.7: Comparison between measured frequency response and predicted response using equation 5.11 with best-fit connection parameters (8,9,10 and 11:1 tools)

5.2.2. The Effect of the Tool Length and Clamping Torque

HSS and carbide end mill with 4 flutes, 20 mm diameter, and 104 mm length are used for test. Different clamping torque values (25 Nm, 35 Nm and 45 Nm) are applied on HSK40 holder. The tool effective diameter was determined as 19.498-mm. Damping

coefficients for HSS and carbide tools were 26 Ns/m and 60 Ns/m, respectively. The nonlinear least square evaluation is used to find the stiffness and damping coefficients for HSS and carbide tool and tool holder/spindle combination. (Table 5.2)

HSS	L/D=4.8	L/D=4.8	L/D=4.8
	D=20, L=96, T=25, $L_{contact}$=8	**D=20, L=96, T=35, $L_{contact}$=8**	**D=20, L=96, T=45, $L_{contact}$=8**
kx (N/m)	$4.46* 10^7$	$5.00* 10^7$	$5.58* 10^6$
kq (Nm/rad)	$3.41* 10^4$	$3.65* 10^4$	$3.98* 10^4$
cx (Ns/m)	1401	1592	1798
cq (Nms/rad)	0.2	0.3	0.4

CARBIDE	L/D=4.8	L/D=4.8	L/D=4.8
	D=20, L=96, T=25, $L_{contact}$=8	**D=20, L=96, T=35, $L_{contact}$=8**	**D=20, L=96, T=35, $L_{contact}$=8**
kx (N/m)	$4.56* 10^7$	$5.27* 10^7$	$5.72* 10^7$
kq (Nm/rad)	$4.12* 10^4$	$4.32* 10^4$	$4.54* 10^4$
cx (Ns/m)	1642	1784	1853
cq (Nms/rad)	0.31	0.4	0.52

Table 5.2: Stiffness/ damping coefficients for 20 mm diameter for different materials and clamping torques

The variation of linear and rotational stiffness and damping coefficients for different clamping torques is shown in Figure 5.8. The stiffness and damping coefficients for the combination HSS tool and tool holder/spindle are a bit less than connection coefficients for the combination carbide tool and tool holder/spindle. As the clamping torque applied on tool holder increases, all coefficients increase.

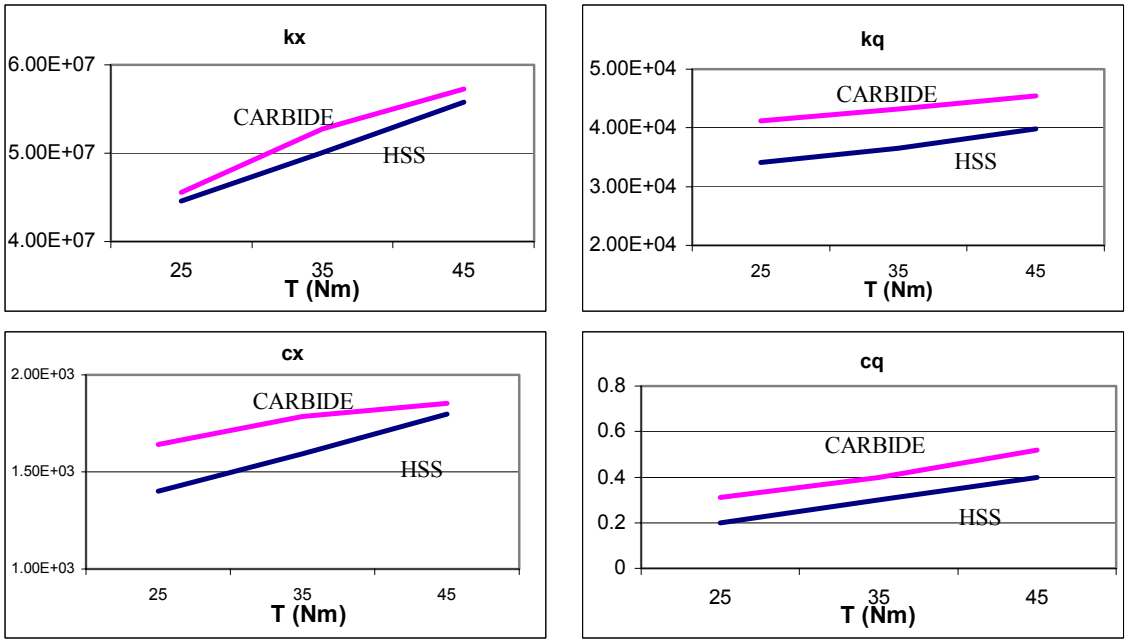

Figure 5.8: Variation of the connection parameters diameter for different materials and clamping torques

Figure 5.9 shows an example of the experimental and predicted direct tool point FRFs (G_{11}) for tool material of HSS and carbide. The overall agreement between the predicted and measured results is good. However, small deviations are also seen. This is attributed in imperfect knowledge of tool geometry, deviations in contact conditions between collet and tool and finite repeatability of the FRF measurement process.

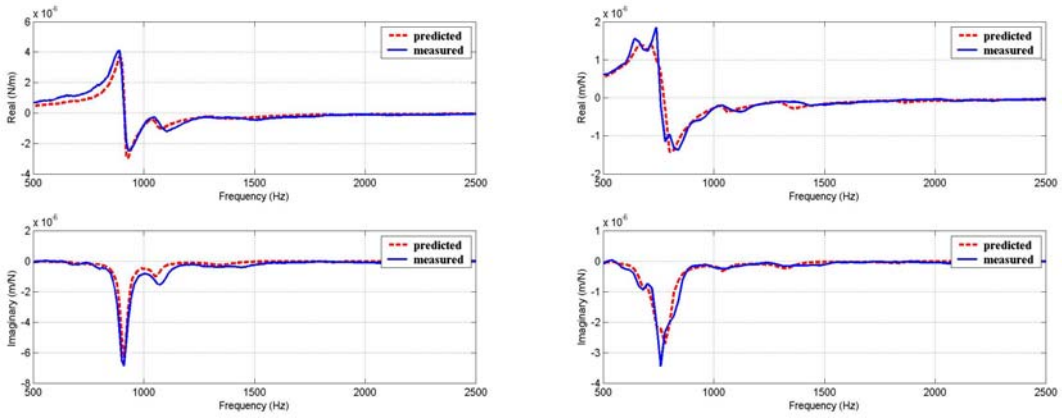

a) HSS b) Carbide

Figure 5.9: Comparison between measured frequency response and predicted response using equation 5.11 with best-fit connection parameters (D=20 mm, L=96 mm, T=35 Nm)

5.2.3. The Interaction between Tool and Tool Holder/Spindle Modes

In the experiment, the HSS end mill, which has 16 mm diameter, 85 mm overhang and 4 flutes, was mounted in HSK40 tool holder. The effective diameter of the end mill and the damping ratio were determined as 15.56 mm and 20 Ns/m, respectively. The linear and rotational spring and damping coefficients for the connection between the tool and tool holder/spindle are given in Table 5.3. The agreement between the predicted and measured results can be seen from the Fig. 5.10**.**

kx (N/m)	kq (Nm/rad)	cx (Ns/m)	cq (Nms/rad)
$84.8* 10^5$	$8* 10^4$	1022	6.3

Table 5.3: Stiffness/ damping coefficients for 16 mm diameter (L/D = 5.3)

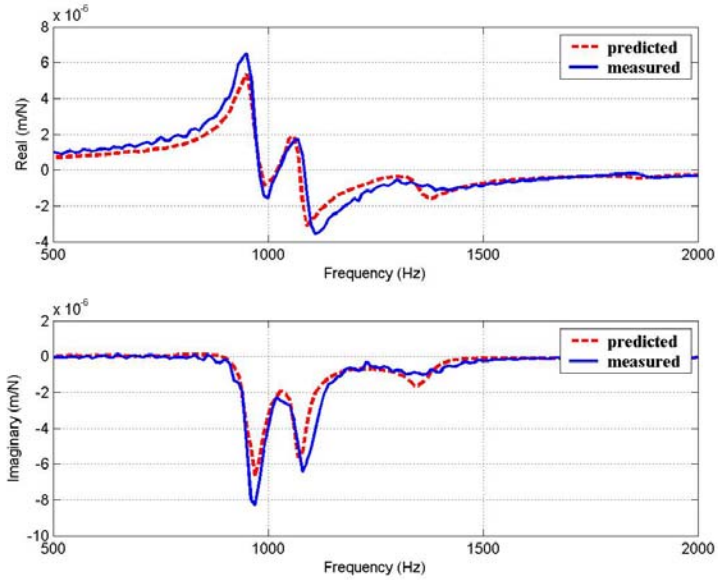

Figure 5.10: Comparison between measured frequency response and predicted response using equation 5.11 with best-fit connection parameters (D=16 mm, L=85 mm, T=45 Nm)

Because of the interaction between tool holder/spindle dynamics and the tool dynamics, two close modes are experienced as shown in the figure. The single tool mode has been effectively split into two dynamically stiffer modes, providing an increase in

stability. This is due to interaction of the cantilever tool mode with approximately 1042 Hz tool holder/spindle mode (Figure 5.2). The analog to this situation is the dynamic absorber, where a small spring/mass is added to a larger vibrating system. The spring constant and mass of the added system are selected such that the natural frequency is equal to excitation frequency of the larger structure and the vibration of the support structure is reduced. Alternatively, this effect may be described as proper impedance matching between the tool and tool holder/spindle substructures.

5.3. Model for Contact Stiffness

The connection between tool and collet is cylindrical. Contact stiffness due to deformations in a connection between two components, tool and tool holder/collet. In cylindrical connections, the radial and angular deformations are important. External forces causes displacements and pressures. The interaction of tool and collet is as shown in Figure 5.11.

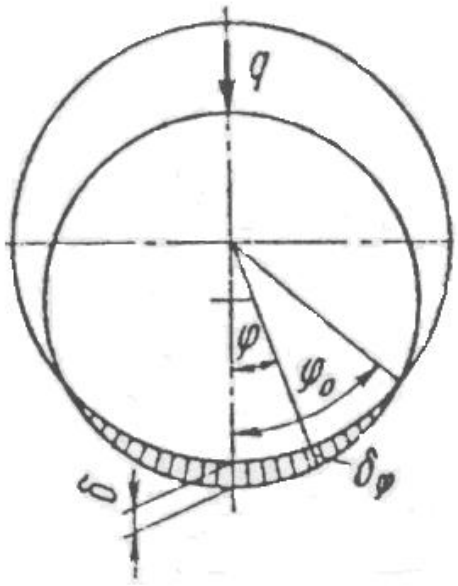

Figure 5.11: Cylindrical connection between tool and tool holder/collet

In the figure, q, in N/m, is load per unit length of connection ($L_{contact}$). Displacement (δ) caused by external force is along the direction of the force. φ_0 is the contact angle. Radial displacement at angle φ is δ_φ.

Under external loading of connection, total pressures on one side are increasing, while on the opposite side they are decreasing. Maximum displacement caused by external force is along the direction of the force, displacement along the circumference can be assumed to be cosinusoidal.

Contact deflections can be considered as proportional to the contact pressure (Rivin, 1999). Two correlations between contact pressure p and deformation δ are considered.

$$\begin{aligned} \delta &= kp \\ \delta &= cp^{0.5} \end{aligned} \tag{5.18}$$

where p is pressure from external load and $k = cp^{-0.5}$ is the contact compliance coefficient. Coefficient c is experimentally determined for different connection materials.

Assuming that interaction of cylinder is as shown in Figure 5.11. There is cosinusoidal load distribution along the arc $2\varphi_0$. Radial displacement at angle φ to the direction of load q:

$$\begin{aligned} \delta_\varphi &= \delta \cos\varphi \\ \delta_\varphi &= kp \cos\varphi \end{aligned} \tag{5.18}$$

Vertical component of contact pressure at angle φ is

$$\begin{aligned} p_\varphi &= p \cos\varphi \\ p_\varphi &= \frac{\delta_\varphi}{k} \cos\varphi = \frac{\delta \cos\varphi}{k} \cos\varphi = \frac{\delta \cos^2 \varphi}{k} \end{aligned} \tag{5.19}$$

The total vertical load can be obtained by integrating p_φ along the contact arc $2\varphi_0$.

$$p = \int_{-\varphi_0}^{\varphi_0} \frac{\delta \cos^2 \varphi}{k} = \frac{\delta}{k} \int_{-\varphi_0}^{\varphi_0} \cos^2 \varphi = \frac{\delta}{2k} \left[\varphi + \cos\varphi \sin\varphi \right]_{-\varphi_0}^{\varphi_0}$$

$$p = \frac{\delta}{k} (\varphi_0 + \cos\varphi_0 \sin\varphi_0) \tag{5.20}$$

$$p = \frac{\delta}{cp^{-0.5}} (\varphi_0 + \cos\varphi_0 \sin\varphi_0)$$

Substitution equation 5.20 into equation 5.18 yields equation 5.21

$$\delta = cp^{0.5} (\varphi_0 + \cos\varphi_0 \sin\varphi_0) \tag{5.21}$$

Stiffness of connection is determined by deformation between the connected surfaces.

$$\frac{qL_{contact}}{\delta} = \frac{qL_{contact}}{c\sqrt{\frac{q}{d}} (\varphi_0 + \cos\varphi_0 \sin\varphi_0)} = C\sqrt{qd}\, L_{contact} (\varphi_0 + \cos\varphi_0 \sin\varphi_0)^{-1}$$

$$k_x = C\sqrt{qd}\, L_{contact} (\varphi_0 + \cos\varphi_0 \sin\varphi_0)^{-1} \tag{5.22}$$

A load and connection stiffness characteristic of the system is nonlinear. *C* is a constant parameter, which changes with material properties (*E*, elastic modulus) of connected parts. The effect of contact length is linear as it is seen in Figure 5.6. The contact angle, φ_0, depends on material properties and clamping torque applied on tool holder. The graph variation of the contact stiffness for different materials (carbide, HSS) and different clamping torques (Figure 5.8) shows the material property and clamping torque effect.

5.4. Summary

The application of receptance coupling substructure analysis (RCSA) to tool point FRF prediction has been demonstrated. The derivation analytical expressions for FRFs, which is coupled with tool holder/spindle experimental FRFs is shown. The method of identification of the connection parameters (stiffness and damping) between tool and tool holder/spindle is presented. The experimental and predicted results are compared. The effects of changes in tool geometric parameters and clamping conditions are explained. The model for contact stiffness is developed.

CHAPTER 6

EXPERIMENTAL APPLICATION

The stiffness and deflection of a cutting tool is very important for accuracy and stability in a machining process. Proper cutting conditions can be selected using the structural characteristics of the cutting system in order to improve quality and productivity. In this chapter, application of the structural modeling methods will be demonstrated by experiments.

Static deformations of the tool are important for machined part precision and surface quality. The stiffness that can be calculated analytically is used to predict the maximum surface error generated by the end mill. In the first section, the analytical displacement and stiffness calculations, which were presented in chapter 3, are verified by experiments where displacement of the tool is measured. The comparison of the experimental and analytic results is presented in the second section.

Dynamic models developed for end mills in this study can be used for transfer function and stability calculations. In the third section, it is demonstrated that the analytical solution can accurately predict the dynamic properties of the tool. In the fourth section, the application of segmented beam formulation is demonstrated for two different beams.

6.1. Stiffness Calculation

Stiffness is the capacity of a mechanical system to sustain loads without excessive changes of its geometry. Stiffness effects on performance of mechanical systems are due to influence of deformations on static strength, wear resistance, efficiency, accuracy, dynamic stability and manufacturability.

The analytical stiffness calculation for cutting tool is explained in chapter 3. End mill is taken as a segmented beam, one segment for the part with flute and the other segment for the shank. Maximum displacement for the end point is given in equation 3.15 according to geometric properties of the tool. Stiffness of the tool can be calculated easily by using maximum displacement. In order to check accuracy of analytic stiffness calculation an experiment was carried out which is presented here.

4-flute high speed steel long slender end mill is selected to demonstrate the accuracy of analytical results. The mill and shank diameter is 6 mm, the flute length is 38 mm and the gauge length is 75 mm. A force (*F*) is applied to end point of the tool and measured by dynamometer (Figure 6.1) Displacements at *X1* and *X2* are measured by dial gage.

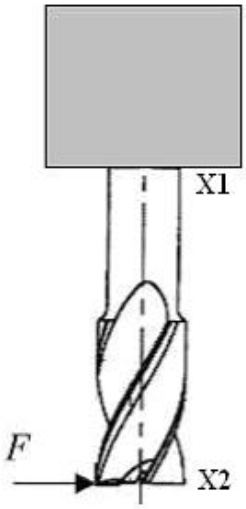

Figure 6.1: Experimental set-up of stiffness measurement

Total displacement of the tool is equal to summation of clamping displacement, beam displacement and rotational displacement. Rotational displacement is assumed to be zero. In order to calculate clamping stiffness the displacement at X1 is also measured. Following figure explains the method used for the calculation.

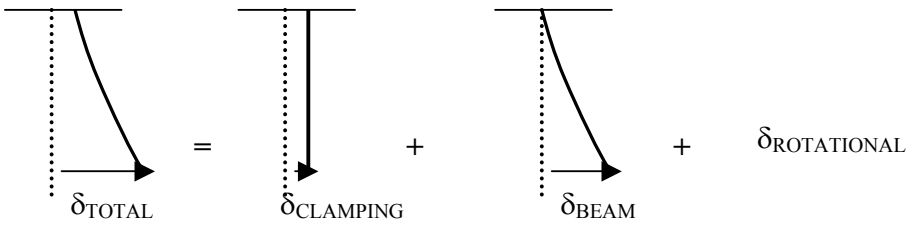

Figure 6.2: Theory of displacement measurement calculation

Force, 28.5 N is applied to the end of the tool. The displacement at X1 and X2 are 0.008 mm and 0.388 mm, respectively. The displacement of the beam is calculated as 0.380 mm. The experimental beam stiffness is 75 N/mm. The analytical maximum displacement of the beam is 0.403 mm according to applied force, 28.5 N. So the stiffness of the tool, which is calculated by using displacement from analytical equation, is 70.5 N/mm. The agreement between two stiffness values is very satisfactory. The small difference may result from experimental errors.

6.2. Maximum Surface Error

Maximum dimensional surface error is obtained from cutting force and surface generation models presented in chapter 2. Maximum surface error varies according to cutting conditions. Therefore, feasible cutting conditions such as radial depth of cut and federate can be determined from maximum surface error data.

The stiffness of an end mill can be calculated using the analytic model presented in chapter 3. The stiffness values are used to predict the maximum surface error generated by the end mill. For surface error calculation, the cutting forces are determined according to work material properties, cutting and tool conditions (Altintas, 2000). The results are verified using the experimental results in (Budak and Altintas, 1994). 4-flute high speed steel end mill with 30^0 helix angle is used for comparision. The tool diameter is 19.05 mm and the tool gauge length is 54.5 mm. The stiffness of this tool is 12761 N/mm. Cutting conditions are summarized in Table 6.1. The cutting forces are determined according to these cutting parameters (Budak and Altintas, 1994).

Cutting pressure coefficient (K_T)	546 MPa
p	0.246
Cutting force coefficient (K_T)	0.270
q	0.271
Entry Angle, Exit angle	0^0, 90^0

Table 6.1: Cutting conditions to calculate the cutting forces and max surface error

The model results agree with the experimental results (Table 6.2). The error in the prediction of the maximum surface error (Emax) is less than % 6.

Axial depth of cut (mm)	Federate (mm/tooth)	Emax Exp. (mm)	Emax Model (mm)	ERROR (%)
19.05	0.14	0.0944	0.0912	3.38
15.00	0.10	0.0722	0.0677	6.23
15.00	0.06	0.0444	0.0438	1.35
15.00	0.02	0.0178	0.0167	6.18
18.00	0.02	0.0166	0.0158	4.82

Table 6.2: Experimental and calculated maximum surface error results

6.3. Chatter Avoidance

Machine tool vibrations are the self exited oscillations of cutting tool and workpiece. In order to generate the stability diagrams dynamic characteristics of the tool is needed. The excessive vibrations of the cutter and workpiece result in poor surface finish and dimensional accuracy and may damage the workpiece and machine tool. Chatter vibration free spindle speeds and axial depth of cuts can be selected from stability chats

Frequency response function (FRF) is required for chatter stability diagrams. In order to obtain the FRF, the tool point is excited using a hammer. This is time consuming for each tool/holder/spindle assembly. The analytic solution is very useful to identify the dynamic properties for especially long tools. The dynamics of tool holder/spindle can be neglected when very tool length is used. A cutting tool can be considered as fixed-free bar as in the analytical solution.

6.3.1. Example 1

4-flute high speed steel end mill with long overhang is selected to demonstrate the accuracy of analytical results. The analytical solution is also compared with cylinder approximation commonly used for end mills. The mill and shank diameter is 12 mm, the flute length is 26 mm and the gauge length is 74 mm. FRF measurement was performed to determine the transfer function of the end mill, which is shown in Figure 6.3. Table 6.3 shows the frequency, stiffness, damping and mass values for the end mill, and the cylinder with the same diameter and length. The graphs between the magnitude of the transfer function and frequency for all methods are shown in Figure 6.3. The approximation results could be improved by using an effective diameter for the cylinder. The analytical solution is the most powerful approximation to find the dynamic properties.

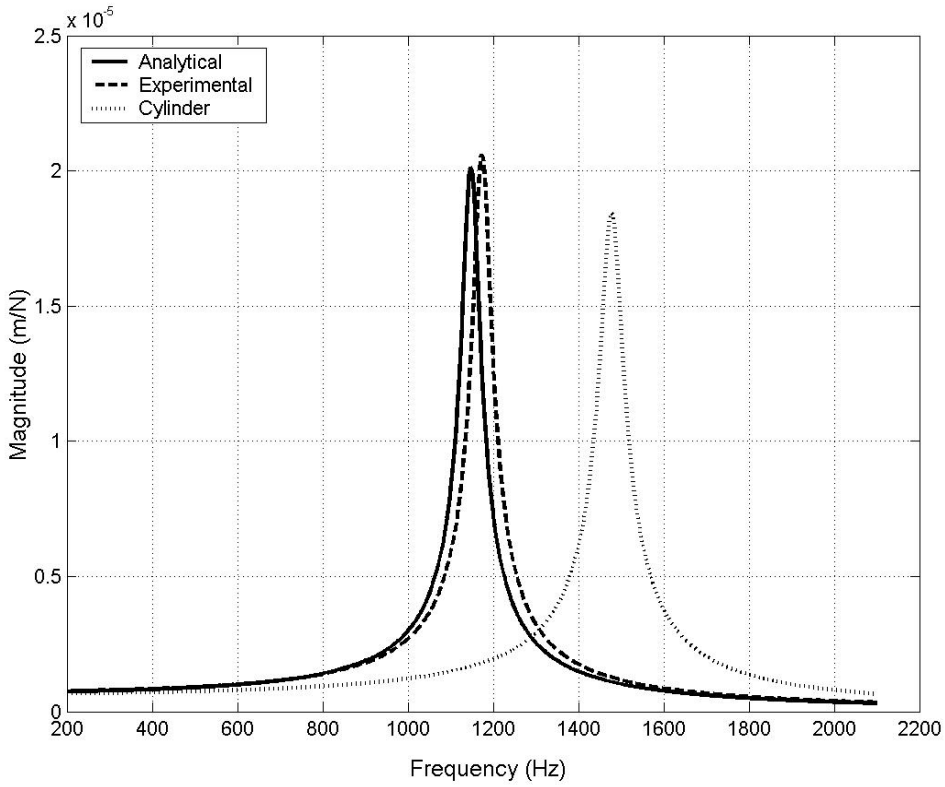

Figure 6.3: Magnitude of the transfer function for the experimental, analytical and cylinder methods for example 1

Transfer Function	Frequency (Hz)	Stiffness (N/m)	Damping (ζ)	Mass (kg)
Experimental	1174	1.35E+6	0.018	0.0250
Analytical	1148	1.38E+6	0.018	0.0265
Cylinder	1478	1.51E+6	0.018	0.0175

Table 6.3: The comparison of the dynamic properties for example 1

The stability lobe for down milling of Al-7075 with radial width of the cut 2.5 mm is determined using the equations described in chapter 4 (CutPro©) (Altintas, 2000) shown in Figure 6.4. The minimum stable depth of cut is 0.2 mm.

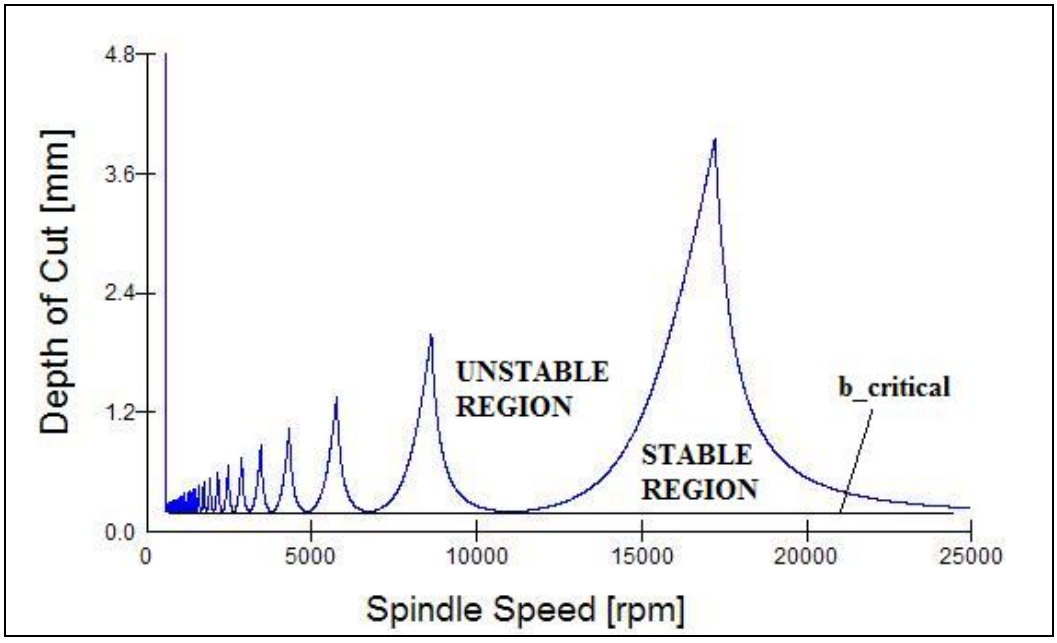

Figure 6.4: Stability lobe diagram for example 1

6.3.2. Example 2

For example 2, HSS end mill, which has 10 mm mill and shank diameter, 22 mm the flute length, 69 mm the gauge length and 4-Flute, was mounted in HSK 40 tool holder. In order to determine the transfer function of the end mill FRF measurement was performed, analytical equations and cylinder approximation are used (Figure 6.5). Table 6.4 shows the frequency, stiffness, damping and mass value for the end mill, which are obtained from experiment and analytical equations, and for the cylinder with the same diameter and length. The most powerful approximation to find the dynamic properties is the analytical solution. When the cylinder approximation is compared with experimental result, it is observed that it is not a very accurate method. The agreement between experimental and analytical results in example 2 is sufficient.

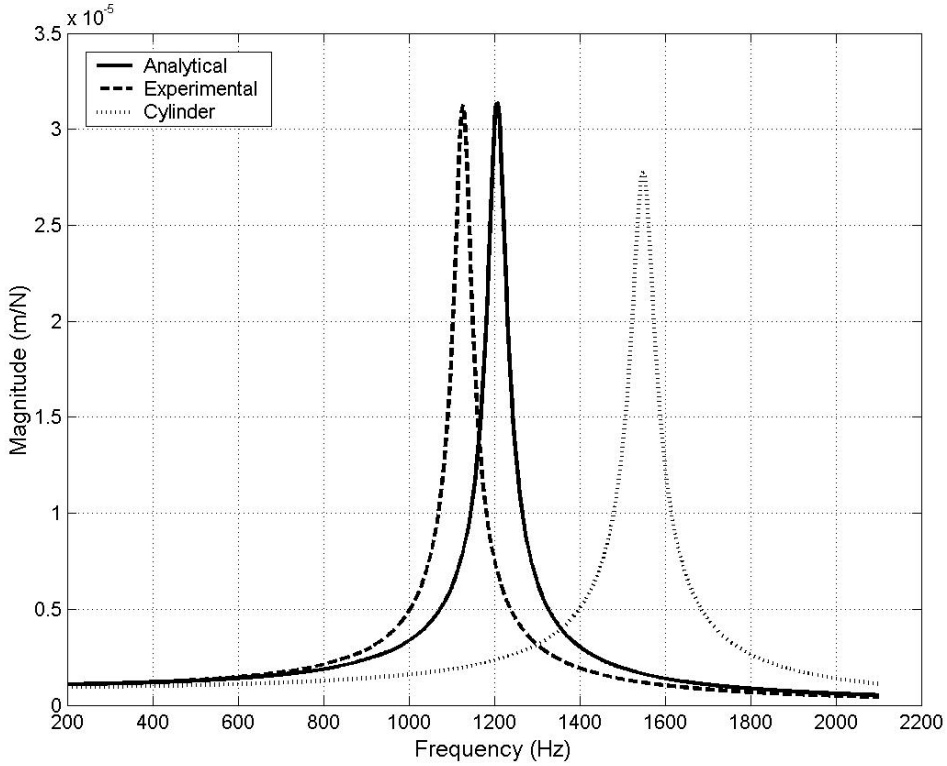

Figure 6.5: Magnitude of the transfer function for the experimental, analytical and cylinder methods for example 2.

Transfer Function	Frequency (Hz)	Stiffness (N/m)	Damping (ζ)	Mass (kg)
Experimental	1127	9.53E+5	0.0168	0.0190
Analytical	1207	9.47E+5	0.0168	0.0165
Cylinder	1549	1.07E+6	0.0168	0.0113

Table 6.4: The comparison of the dynamic properties for example 2

The stability lobe for down milling of Al-7075 with radial width of the cut 2.5 mm is determined and shown in Figure 6.6. The minimum stable depth of cut is 0.1 mm for example 2.

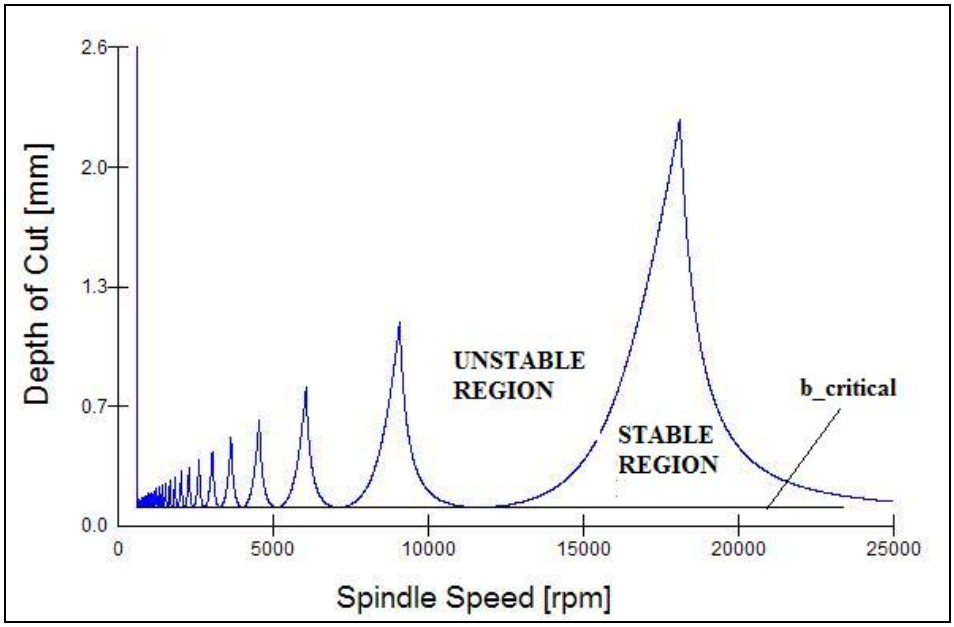

Figure 6.6: Stability lobe diagram for example 2

6.4. Application of Segmented Beam Formulation

The determination of fundamental natural frequency for segmented beam is explained in chapter 4. Because of the complex matrix calculations (equation 4.13), the determination of natural frequency is very difficult. Therefore, a graph was created based on the geometric properties of the beam. From this graph (Figure 4.2) *K* value can be selected to calculate natural frequency. Then, simplified equations were developed according to length ratio (*L1/L2*) and diameter ratio (*D1/D2*) (equation 4.18). Fundamental natural frequency can be easily calculated by using *K* value, geometric properties and material properties (equation 4.17).

For this section, two segmented beams, which have different materials and geometric properties, are selected (Figure 6.7). In this analysis, the length and diameter ratios are more important than the exact length diameter values. The mechanical properties of the material are given in Table 6.5 (Beer and Johnston, 1992).

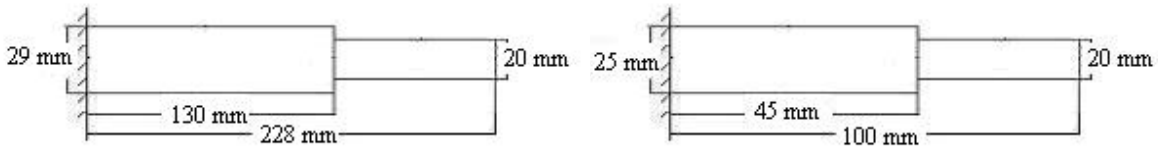

a) Aluminum beam b) Steel beam

Figure 6.7: Geometric properties of aluminum and steel segmented beams

MATERIAL	Elastic Modulus (GPa)	Density (kg/m^3)
Steel	200	7860
Aluminum	72	2800

Table 6.5: Mechanical properties of the segmented beam materials

The *K* value is calculated from the matrix solution (equation 4.13), the graph (Figure 4.2) and the simplified equations (equation 4.18). Following calculation shows the K value determination from simplified equations for aluminum segmented beam. Table 6.6 shows all K values for three different methods.

$$K = \frac{1}{a\left(\frac{D1}{D2}\right)+b},\ a = \frac{-0.817(\ln l)+0.0167}{l},\ b = 0.1821l^2 + 0.1063l - 0.0275$$

$$l = \frac{L1}{L2} = 0.57, \frac{D1}{D2} = 1.45 \rightarrow K = 0.767$$

K	MATRIX	GRAPH	EQUATION
L1/L2=0.57, D1/D2=1.45, Aluminum	0.808	0.790	0.767
L1/L2=0.31, D1/D2=1.25 Steel	0.271	0.260	0.253

Table 6.6: K values for three different methods of natural frequency calculation

Material properties, geometric properties and *K* values for all methods are substituted into equation 4.17 and natural frequency is calculated. Following calculation demonstrates natural frequency of the aluminum segmented beam.

$$\omega_{matrix} = \frac{0.808}{2\pi}\sqrt{\frac{72.10^9\,\frac{\pi(0.029)^4}{64}}{2800\frac{\pi(0.029)^2}{4}(0.130)^4}} = 279 \quad \text{Hz}$$

$$\omega_{graph} = \frac{0.790}{2\pi}\sqrt{\frac{72.10^9\,\frac{\pi(0.029)^4}{64}}{2800\frac{\pi(0.029)^2}{4}(0.130)^4}} = 273 \quad \text{Hz}$$

$$\omega_{equation} = \frac{0.767}{2\pi}\sqrt{\frac{72.10^9\,\frac{\pi(0.029)^4}{64}}{2800\frac{\pi(0.029)^2}{4}(0.130)^4}} = 265 \quad \text{Hz}$$

Experimental modal analysis results (Figure 6.8) for two aluminum and steel segmented beams and the frequencies, which are calculated from matrix, graph and simplified equations, are tabulated in Table 6.7.

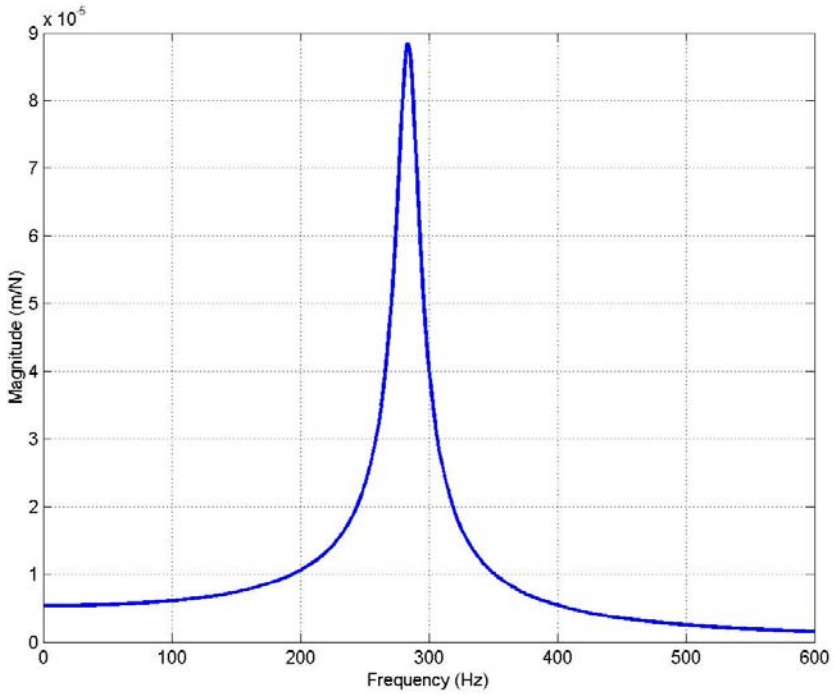

Figure 6.8: The experimental FRF measurement for aluminum segmented beam

FREQUENCY (Hz)	MATRIX	GRAPH	EQUATION	EXPERIMENT
L1/L2=0.57, D1/D2=1.45 Aluminum	279	273	265	284
L1/L2=0.31, D1/D2=1.25 Steel	671	651	627	693

Table 6.7: Frequency results from experiments and other methods

Obviously, the frequency, which is calculated from complex matrix equations, is very close to the experimentally determined frequency. Instated of using the graph for the *K* value, using the simplified equations is much easier. However, the error of the frequency of

the simplified equations is more than the frequency of the graph method. (% 6.6 for aluminum segmented beam and %9.5 for steel segmented beam)

After determining the natural frequency, the mode shape can be obtained by using arbitrary constant vector *A* from equation (4.12). The mode shape, which is obtained by using the solution for matrix equations for aluminum beam, is given in Figure 6.9.

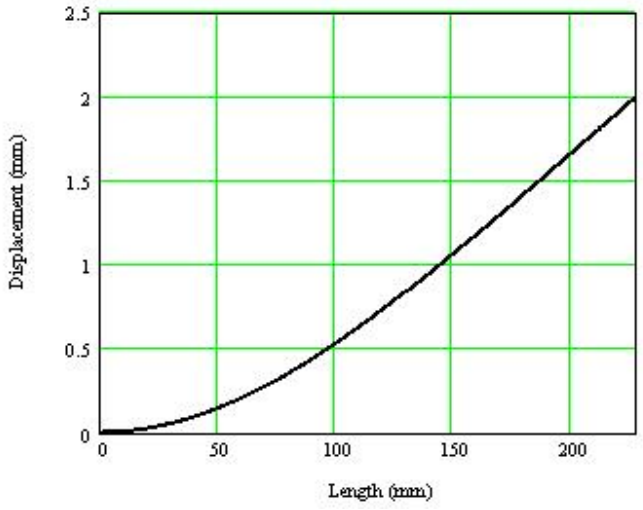

Figure 6.9: Mode shape for the solution of matrix equations

For the first bending mode, maximum displacement occurs at the end of the beam. The comparison of the mode shapes of the aluminum segmented beam for all three methods is given in Table 6.8. The table contains the ratio of displacement at certain point and maximum displacement.

Displacement / Max Displacement	**at 50 mm**	**at 100 mm**	**at 150 mm**	**at 200 mm**	**at 228 mm**
MATRIX	0.07325	0.26597	0.53145	0.82955	1
GRAPH	0.07579	0.27009	0.53515	0.83095	1
EQUATION	0.07896	0.27526	0.53975	0.8327	1

Table 6.8: The comparison of the mode shapes for three different methods

6.5. Summary

Applications of the models are demonstrated by 4 examples. The first one is on prediction of the deflection and stiffness of the tool. Then, the prediction of the form error due to tool deflection is demonstrated in the second example. The third one is on the prediction of the tool transfer function, which is required for chatter avoidance and stability limit calculations. Finally, the application of the simplified segmented beam equations is demonstrated with examples.

CHAPTER 7

CONCLUSION

In this study, generalized equations are presented which can be used for predicting the static and dynamic properties of milling system components. Both FEA and analytical methods have been used for static and dynamic analysis of end mills. The results are verified experimentally. RCSA model has been used for combining the measured dynamics of the tool holder/spindle and the analytically determined end mill modes. The connection parameters between tool and tool holder/spindle are identified.

Dynamic and static properties of milling tools are very important for machining precision and chatter stability. In general, approximate analytical or experimental results are used to determine these characteristics. Approximate results do not provide accurate information particularly for the dynamics and chatter stability. Experimental methods, on the other hand, are time consuming considering the possible number of tool and tool holder combinations, tool geometry and material in an industrial setting. The analytical models presented in this work eliminate measurements for every tool assembly. The models consider the complex geometry of flutes in development of cross sectional properties. The approach presented here is very useful for implementation in a virtual machining system where the form errors and stability limits for a milling application can be determined automatically.

End mills have flutes and unfluted sections, which further complicate their geometry. This segmented characteristic has also been considered in static and dynamic modeling. This is an original contribution of this work. Simplified equations for segmented beam can be used for any area. Due to its wide use in industry, milling process is considered, however the same methods can be applied to other machining operations as well.

As a future work the modeling of contact parameters will be developed. The parameters can be determined by using these models according to tool geometric conditions, material properties and clamping force. In the future, all study, which is done for tool and tool holder, can be done for spindle and machine. All models can be integrated into CAD/CAM systems to develop a virtual machining system for precision machining.

REFERENCES

1. Altintas, Y. and Lee, P. ,1996, A general mechanics and dynamics model for helical end mills. Annals of the CIRP, 45 : 59-64.

2. Altintas, Y. and Engin, S., 2001, Generalized modeling of mechanics and dynamics of milling cutters, Annals of the CIRP, 50: 25-30.

3. Altintas, Y., 2000, Manufacturing Automation, Cambridge University Press.

4. Altintas, Y., 2000, Modeling Approaches and Software for Predicting the Performance of Milling Operations at MAL-UBC, Machining Science and Technology, 4/3: 445-478.

5. Altintas, Y. and Spence, A., 1991, End Milling Force Algorithms for CAD Systems, Annals of the CIRP, 40:31-34.

6. Aoyama, T., Inasaki, I., 2001, Performances of the HSK Tool interfaces under High Rotational Speed, Annals of the CIRP, 50/1:281-284.

7. Armarego, E.J.A. and Whitfield, R.C., 1985, Computer based modeling of popular machining operations for force and power predictions. Annals of the CIRP, 34 : 65-69.

8. Beer, F., Johnston, E., 1992, Mechanics of Materials, Mcgraw-Hill , U.K.

9. Bishop, R.E.D. and Johnson, D.C., 1960, The Mechanics of Vibration, Cambridge University Press, Cambridge, U.K.

10. Budak, E., 1994, The Mechanics and Dynamics of Milling Thin-Walled Structures, Ph.D. Dissertation, University of British Columbia.

11. Budak, E. and Altintas, Y., 1994, Identification of Peripheral Milling Conditions for Improved Dimensional Accuracy, Int.J. Machine Tools and Manufacture, 34/ 7:907-918.

12. Budak, E. and Altintas, Y., 1995, Modeling and avoidance of static deformations in peripheral milling of plates. International Journal of Machine Tools and Manufacture, 34/ 3:459-476.

13. Budak, E., Altintas, Y. and Armarego, E.J.A., 1996, Prediction of Milling Force Coefficients From Orthogonal Cutting Data, Trans. ASME Journal of Manufacturing Science and Engineering, 118:216-224.

14. Budak,E. and Altintas, Y. , 1998, Analytical prediction of chatter stability in milling-Part I: General formulation; Part II: Application to common milling systems. Trans. ASME, Journal of Dynamic Systems, Measurement, and Control, 120:22-36.

15. Budak, E., 2002, Modeling End Milling Process Including Part-Tool Flexibility and Dynamics", Proceedings of 3rd International Seminar on Intelligent Computation in Manufacturing Engineering (ICME 2002), 243-250, Ischia, Italy.

16. Chaudhari, t. and Maiti S., 2000, A study of geometrically segmented beams with and without crack, Int. Journal of Solids and Structures, 37:61-779

17. Duncan, W.J., Mechanical Admittances and their Applications to Oscillation Problems, 1947, Ministry of Supply, Aeronautical Research Council Reports and Memoranda No. 2000, London: His Majesty's Stationery Office.

18. Ewins, D.J., 1986, Analysis of Modified or Coupled Structures Using FRF Properties, Imperial College London, Dynamics Section, Mechanical Engineering, Report No. 86002.

19. Ferreira, J., and Ewins, D., 1995, Nonlinear Receptance Coupling Approach Based on Describing Functions, Proceedings of the 14th International Modal Analysis Conference, Dearborn, Michigan, 1034-1040.

20. Jorgensen, B., Shin, Y., 1998, Dynamics of Spindle-Bearing Systems at High Speeds Including Cutting Load Effects, Trans. ASME Journal of Manufacturing Science and Engineering, 120/2:387-394.

21. Kivanc, E., Budak, E., 2003, Proceeding of Modelling Statics and Dynamics of Milling System Components, Proceedings of the CIRP International Seminar on Manufacturing Systems, Saarbrucken, Germany.

22. Kline, W.A., DeVor, R.E., and Shareef, I.A., 1982, The prediction of surface accuracy in end milling. Trans ASME Journal of Engineering for Industry, 104 : 272-278.

23. Koenigsberger, F. and Sabberwal, A.J.P., 1961, An investigation into the cutting force pulsations during milling operations. International Journal of Machine Tool Design and Research, 1:15-33.

24. Koenigsberger, F. and Tlusty, J., 1967, Machine Tool Structures-Vol. I: Stability Against Chatter, Pergamon Press.

25. Kops, L. and Vo, D., 1990, Determination of the Equivalent Diameter of an End Mill Based on Its Compliance, Annals of the CIRP, 39:93-96.

26. Nermes, J.A, Asamoah-Attiah, S., Budak, E., 2001, Cutting Load Capacity of End Mills with Complex Geometry, Annals of the CIRP, 50/1:65-68.

27. MathWorks, 2002, Mathlab 6.5.0 Relase 13: High Performance Numeric Computation and Visualization Software, Naatick, Massachusetts.

28. Park, S., Altintas, Y., Movahhedy, M. ,2003, Receptance Coupling for end mills, International Journal of Machine Tools & Manufacture, 43:889-896.

29. Rivin, Eugene, 2001, Stiffness and Damping in Mechanical Design, Marcel Dekker Press, USA

30. Rao, S., 1995, Mechanical Vibrations, Addison Wesley.

31. Smith, S. and Tlusty, J., 1991, An overview of modeling and simulation of the milling process. Trans. ASME Journal of Engineering for Industry, 13 :169-175

32. Smith, S., Winfough, W., and Halley, J., 1998, The Effect of Tool Length on Stable Metal Removal Rate in High-Speed Milling, Annals of the CIRP, 47/1: 307–310.

33. Schmitz, T., and Donaldson, R., 2000, Predicting High-Speed Machining Dynamics by Substructure Analysis, Annals of the CIRP., 49/ 1:303–308.

34. Schmitz, T., Davies, M., Kennedy, M., 2001, Tool Point Frequency response Function For High Speed Machining by RCSA, ASME, 123: 700-707

35. Schmitz, T., Burns, 2003, Receptance Coupling for High Speed Machinig Dynamics Prediction, Proceedings of the 2003 International Modal Analysis Conference (IMAC-XXI), Kissimmee, FL.

36. Shih, R., 2000, Introduction to Finite Element Analysis, SDC

37. Tlusty, J. and Polacek, M., 1963, The Stability of Machine Tools Against Self Excited Vibrations in Machining, International Research in Production Engineering ASME, 465-474

38. Tobias, S.A., 1965, Machine Tool Vibration, Blackie and Sons Ltd

39. Weck, M., Altintas, Y. and Beer, C., 1994, CAD Assisted Chatter Free NC Tool Path Generation in Milling, International Journal of Machine Tools and Manufacture, 34:879-891

40. Yazar, Z., Koch, K.F., Merrick, T. and Altan, T., 1994, Feed Rate Optimization Based on Cutting Force Calculations in 3-Axis Milling of Dies and Molds with Sculptured Surfaces, Int. Journal of Machine Tools and Manufacture, 34/3:365-377.

REFERENCES

1. Altintas, Y. and Lee, P. ,1996, A general mechanics and dynamics model for helical end mills. Annals of the CIRP, 45 : 59-64.

2. Altintas, Y. and Engin, S., 2001, Generalized modeling of mechanics and dynamics of milling cutters, Annals of the CIRP, 50: 25-30.

3. Altintas, Y., 2000, Manufacturing Automation, Cambridge University Press.

4. Altintas, Y., 2000, Modeling Approaches and Software for Predicting the Performance of Milling Operations at MAL-UBC, Machining Science and Technology, 4/3: 445-478.

5. Altintas, Y. and Spence, A., 1991, End Milling Force Algorithms for CAD Systems, Annals of the CIRP, 40:31-34.

6. Aoyama, T., Inasaki, I., 2001, Performances of the HSK Tool interfaces under High Rotational Speed, Annals of the CIRP, 50/1:281-284.

7. Armarego, E.J.A. and Whitfield, R.C., 1985, Computer based modeling of popular machining operations for force and power predictions. Annals of the CIRP, 34 : 65-69.

8. Beer, F., Johnston, E., 1992, Mechanics of Materials, Mcgraw-Hill , U.K.

9. Bishop, R.E.D. and Johnson, D.C., 1960, The Mechanics of Vibration, Cambridge University Press, Cambridge, U.K.

10. Budak, E., 1994, The Mechanics and Dynamics of Milling Thin-Walled Structures, Ph.D. Dissertation, University of British Columbia.

11. Budak, E. and Altintas, Y., 1994, Identification of Peripheral Milling Conditions for Improved Dimensional Accuracy, Int.J. Machine Tools and Manufacture, 34/ 7:907-918.

12. Budak, E. and Altintas, Y., 1995, Modeling and avoidance of static deformations in peripheral milling of plates. International Journal of Machine Tools and Manufacture, 34/ 3:459-476.

13. Budak, E., Altintas, Y. and Armarego, E.J.A., 1996, Prediction of Milling Force Coefficients From Orthogonal Cutting Data, Trans. ASME Journal of Manufacturing Science and Engineering, 118:216-224.

14. Budak,E. and Altintas, Y. , 1998, Analytical prediction of chatter stability in milling-Part I: General formulation; Part II: Application to common milling systems. Trans. ASME, Journal of Dynamic Systems, Measurement, and Control, 120:22-36.

15. Budak, E., 2002, Modeling End Milling Process Including Part-Tool Flexibility and Dynamics", Proceedings of 3rd International Seminar on Intelligent Computation in Manufacturing Engineering (ICME 2002), 243-250, Ischia, Italy.

16. Chaudhari, t. and Maiti S., 2000, A study of geometrically segmented beams with and without crack, Int. Journal of Solids and Structures, 37:61-779

17. Duncan, W.J., Mechanical Admittances and their Applications to Oscillation Problems, 1947, Ministry of Supply, Aeronautical Research Council Reports and Memoranda No. 2000, London: His Majesty's Stationery Office.

18. Ewins, D.J., 1986, Analysis of Modified or Coupled Structures Using FRF Properties, Imperial College London, Dynamics Section, Mechanical Engineering, Report No. 86002.

19. Ferreira, J., and Ewins, D., 1995, Nonlinear Receptance Coupling Approach Based on Describing Functions, Proceedings of the 14th International Modal Analysis Conference, Dearborn, Michigan, 1034-1040.

20. Jorgensen, B., Shin, Y., 1998, Dynamics of Spindle-Bearing Systems at High Speeds Including Cutting Load Effects, Trans. ASME Journal of Manufacturing Science and Engineering, 120/2:387-394.

21. Kivanc, E., Budak, E., 2003, Proceeding of Modelling Statics and Dynamics of Milling System Components, Proceedings of the CIRP International Seminar on Manufacturing Systems, Saarbrucken, Germany.

22. Kline, W.A., DeVor, R.E., and Shareef, I.A., 1982, The prediction of surface accuracy in end milling. Trans ASME Journal of Engineering for Industry, 104 : 272-278.

23. Koenigsberger, F. and Sabberwal, A.J.P., 1961, An investigation into the cutting force pulsations during milling operations. International Journal of Machine Tool Design and Research, 1:15-33.

24. Koenigsberger, F. and Tlusty, J., 1967, Machine Tool Structures-Vol. I: Stability Against Chatter, Pergamon Press.

25. Kops, L. and Vo, D., 1990, Determination of the Equivalent Diameter of an End Mill Based on Its Compliance, Annals of the CIRP, 39:93-96.

26. Nermes, J.A, Asamoah-Attiah, S., Budak, E., 2001, Cutting Load Capacity of End Mills with Complex Geometry, Annals of the CIRP, 50/1:65-68.

27. MathWorks, 2002, Mathlab 6.5.0 Relase 13: High Performance Numeric Computation and Visualization Software, Naatick, Massachusetts.

28. Park, S., Altintas, Y., Movahhedy, M. ,2003, Receptance Coupling for end mills, International Journal of Machine Tools & Manufacture, 43:889-896.

29. Rivin, Eugene, 2001, Stiffness and Damping in Mechanical Design, Marcel Dekker Press, USA

30. Rao, S., 1995, Mechanical Vibrations, Addison Wesley.

31. Smith, S. and Tlusty, J., 1991, An overview of modeling and simulation of the milling process. Trans. ASME Journal of Engineering for Industry, 13 :169-175

32. Smith, S., Winfough, W., and Halley, J., 1998, The Effect of Tool Length on Stable Metal Removal Rate in High-Speed Milling, Annals of the CIRP, 47/1: 307–310.

33. Schmitz, T., and Donaldson, R., 2000, Predicting High-Speed Machining Dynamics by Substructure Analysis, Annals of the CIRP., 49/ 1:303–308.

34. Schmitz, T., Davies, M., Kennedy, M., 2001, Tool Point Frequency response Function For High Speed Machining by RCSA, ASME, 123: 700-707

35. Schmitz, T., Burns, 2003, Receptance Coupling for High Speed Machinig Dynamics Prediction, Proceedings of the 2003 International Modal Analysis Conference (IMAC-XXI), Kissimmee, FL.

36. Shih, R., 2000, Introduction to Finite Element Analysis, SDC

37. Tlusty, J. and Polacek, M., 1963, The Stability of Machine Tools Against Self Excited Vibrations in Machining, International Research in Production Engineering ASME, 465-474

38. Tobias, S.A., 1965, Machine Tool Vibration, Blackie and Sons Ltd

39. Weck, M., Altintas, Y. and Beer, C., 1994, CAD Assisted Chatter Free NC Tool Path Generation in Milling, International Journal of Machine Tools and Manufacture, 34:879-891

40. Yazar, Z., Koch, K.F., Merrick, T. and Altan, T., 1994, Feed Rate Optimization Based on Cutting Force Calculations in 3-Axis Milling of Dies and Molds with Sculptured Surfaces, Int. Journal of Machine Tools and Manufacture, 34/3:365-377.